INVESTIGATION OF EXPERIMENTAL VARIATION OF BOVINE SPHINGOMYELIN AS A NOVEL INGREDIENT FOR ULTRAVIOLET PROTECTION

A Thesis

presented to

the Faculty of California Polytechnic State University,

San Luis Obispo

In Partial Fulfillment

of the Requirements for the Degree

Master of Science in Biomedical Engineering

by

Esther Natalie Chen

June 2020

COMMITTEE MEMBERSHIP

TITLE:	Investigation of Experimental Variation of Bovine Sphingomyelin as a Novel Ingredient for Ultraviolet Protection
AUTHOR:	Esther Natalie Chen
DATE SUBMITTED:	June 2020
COMMITTEE CHAIR:	Lily Hsu Laiho, Ph.D. Professor of Biomedical Engineering
COMMITTEE MEMBER:	David Clague, Ph.D. Professor of Biomedical Engineering
COMMITTEE MEMBER:	Michael Whitt, Ph.D. MBA Professor of Biomedical Engineering

ABSTRACT

Investigation of Experimental Variation of Bovine Sphingomyelin as a Novel Ingredient for Ultraviolet Protection

Esther Natalie Chen

Skin cancer is a prevalent disease that globally affects 2-3 million people per year [1]. This number is expected to grow tenfold as depletion of the ozone layer contributes to harsher rays reaching Earth's surface [2]. A common way to protect against those ultraviolet waves is to apply sunscreen, however, recent reports call into question the safety of some active ingredients as they can enter through the skin into the bloodstream [3]. This thesis aims to investigate an alternative solution that uses bovine sphingomyelin (BSM) as photoprotective solution against UV irradiation.

In order to evaluate the effectiveness of BSM against UV radiation, p21 intensity was measured on a monolayer of keratinocytes, as the intensity directly correlates to cell damage. Additionally, fluorescent sphingomyelin (FSM) was added as a treatment because it was created to be an analog to BSM and allowed for visualization of sphingomyelin within the cell.

Differences in p21 intensities were observed with BSM and FSM showing a reduced p21 intensity compared to the no sphingomyelin case. FSM helped locate sphingomyelin within the cell and a mechanism was proposed for how it reduces cell damage. Lastly, high variation was seen between experimental designs. Further measures were needed to reduce this intra-subject standard deviation, so additional experimental parameters were tested such as min/max intensity values, cell count, and nucleus circularity to explain this variation.

Keywords: Sphingomyelin, Fluorescent Sphingomyelin, p21, UV, Keratinocytes, Variability

ACKNOWLEDGMENTS

This thesis is a cumulation of my studies at Cal Poly as well as all the internships, co-ops, and projects I have had over the last 6 years. I would like to thank my wonderful family – Erlyana, Jusak, and Daniel – for all the support and advice you have given me throughout the years. Their constant optimism and encouragement have shaped me to becoming an independent, confident individual. A huge thanks goes to my advisor, Professor Lily Laiho, for all the guidance and discussions we have had. She gave the courage to pursue this master's degree and she is someone I really admire. Another thanks goes to my tireless, mighty lab partner, Jennifer Kandell for training me, culturing my cells, and advising me through all my experiments. Lastly, I am grateful for all friends and professors that have given me mentorship and support to finish this thesis.

TABLE OF CONTENTS

Page

LIST OF TABLES

LIST OF FIGURES

Figure Page

1 INTRODUCTION

Skin cancer is a prevalent disease that has been on the rise over the past decade. In 2017, there were approximately 2-3 million non-melanoma skin cancer and 132,000 melanoma skin cancer cases globally [1]. Scientists predict that with the depletion of the ozone level, cases of skin cancer will continue to rapidly increase [2]. Currently, the FDA recommends sunscreen as a method of preventative care against skin cancer [2]. However, the safety of sunscreens are being called into question. In a memo published in January 2020, the FDA confirmed evidence that some active ingredients were absorbed through the skin and measured in blood levels [3]. Alternative methods for UV protection are needed and are the motivations for this investigation.

Sphingomyelin is an important class of phospholipids found in most eukaryotic cells [4]. It is postulated that introduction of bovine sphingomyelin can provide protective effects from UV photodamage; however, the exact mechanism is still unknown [5]. P21 is a cyclin-dependent kinase inhibitor that promotes cell cycle arrest in response to many stimuli, one being the phosphorylation of sphingomyelin to ceramide [6]. Cell cycle arrest can lead to DNA repair or apoptosis, but ultimately it helps the maintenance of the genomic integrity [7]. Typically p21 is found within cytoplasm, but will be present in the nucleus after cell damage [5].The presence of p21 in the nucleus helps quantify the cells that have taken UV damage. Using p21 as a cell damage indicator, we hypothesize that bovine sphingomyelin will reduce the cell damage. A series of experiments were designed to help understand sphingomyelin's mechanism and to observe these photoprotective effects.

The overall goals of this thesis were to investigate the protective effects of sphingomyelin by observing differences in cell damage for cells exposed to sphingomyelin compared to those without, to visualize sphingomyelin within the cell, and to identify experimental parameters that could contribute to variation within results.

2 BACKGROUND

2.1 Layers of the Skin

The skin is made of two main layers: dermis and epidermis [8]. The dermis is made of dense, irregular connective tissue that is responsible for autonomic and sympathetic communication to and from the brain [9]. It also contains blood vessels, hair follicles, and sweat glands [9]. The epidermis functions as a waterproof barrier against the outside environment [10]. It contains three main types of cells that may become cancerous: squamous cells, basal cell, and melanocytes [11]. Keratinocytes can be found in both dermis and epidermis layers except at the stratum basale [11].

2.1.1 Dermis

The dermis is mainly responsible for supporting the epidermis; it is composed the papillary dermis and the reticular dermis [12]. The papillary dermis is more superficial and contains capillaries, elastic fibers, reticular fibers, and collagen [12]. The reticular dermis contains blood vessels, interlaced elastic fibers, collagen fibers in parallel layers, fibroblasts, mast cells, nerve endings, and lymphatics [12]. The types of cells in the dermis are fibroblasts, mast cell, and vascular smooth muscle cells [12].

2.1.2 Epidermis

The epidermis of thick skin has five layers (listed from innermost to outermost layer): stratum basale, stratum spinosum, stratum granulosum, stratum lucidum, and stratum corneum [13]. Within those layers, there are four types of cells: keratinocytes, melanocytes, Langerhans, and Merkel cells. Keratinocytes originate in the stratum basale and differentiate up to the stratum corneum; they are responsible for synthesis of keratin [13]. Melanocytes are found in the stratum basale and produce melanin, which is

responsible for hair and skin color as well as protect the living cells from ultraviolet (UV) radiation damage [8]. Langerhan cells originate from bone marrow and are found in the epidermis to detect foreign particles [13]. Lastly, Merkel cells are found in the epidermis of specific areas of the skin, such as nail beds or genitalia, to heighten sensitivity [13].

2.1.3 Keratinocytes

Epidermal keratinocytes are responsible for separating an organism from their environment by producing keratin, an intermediate filament protein [14]. They start in the innermost stratum; these are called basal cells and they can either stay to replenish the population basal keratinocytes or start differentiation [15]. The differentiating cells are called prickle cells and are pushed outward until they reach the stratum spinosum layer [15]. They continue to travel outward to the stratum granulosum and become granular cells [15]. At this point, the cell organelles and nucleus degrade and form a highly keratinized squamous layer called squames which eventually flake off as dead skin cells [15].

2.2 Types of Skin Cancer

Skin cancer is the most common type of cancer worldwide [16]. One in 5 Americans will develop skin cancer by the age of 70 [16]. Skin cancer is classified into nonmelanoma skin cancer and melanoma. The most common types of the nonmelanoma skin cancer are basal cell carcinoma and squamous cell carcinoma [17].

2.2.1 Nonmelanoma Skin Cancer

The main difference between nonmelanoma and melanoma cancer is with the location or type of cells that are malignant [18]. Melanoma begins in the innermost layer

below the stratum basale of the epidermis while nonmelanoma grows in the middle and upper layer of the epidermis such as the stratum granulosum [18].

Basal cell carcinoma (BCC) is the most common form of nonmelanoma skin cancer, mainly caused by acute sun exposure [16]. BCC forms in the basal cells found in the stratum basale of the epidermis [18]. There is an increased risk for light-complexioned people who have painful sunburns with no tanning during exposure to sunlight [19]. There are five main types of BCC: nodulo-ulcerative, pigmented, cystic, superficial, and sclerosing; they are categorized by appearance and location [19].

Squamous cell carcinoma (SCC) is due to the malignant proliferation of epidermal keratinocytes, mainly due to chronic long term solar exposure [19]. SCC forms in squamous cells found in the upper layer of the epidermis [18]. There is higher incidence for organ transplant patients to develop SCC due to increased risk factors such as immunosuppressive therapy, genetic factors, and skin cancer transmission before transplantations [20].

BCC and SCC both grow in a continuous, cellular structure that appear like narrow cellular strands [18]. They are less likely to spread to other parts of the body and can usually be cured if identified and treated early [18]. Typical treatments involve encompassing the entire tumor and eradicating the cancer with the least inconvenience to the patient [21]. Some common treatments include excision, Mohs surgery, electric cauterization, cryotherapy, and laser treatment [22].

2.2.2 Melanoma

Melanoma is when melanocytes start to grow uncontrollably and can metastasize to other parts of the body [23]. Compared to BCC and SCC, melanoma is harder to treat and is responsible for three out of every four deaths caused by skin cancer [24]. Phenotypes with higher risk of melanoma are those with fair skin, fair or red hair, tendency to freckle, and tendency to burn rather than tan [24]. Similar BCC, acute sun exposure is more highly associated with melanoma risk rather than chronic exposure [24]. Diagnosis is dependent on location and its growth pattern; there are five main types: Lentigo maligna melanoma (LMM), superficial spreading melanoma (SSM), nodular melanoma (NM), acral lentiginous melanoma (ALM), and mucosal melanoma (MCM) [24].

2.3 Sunscreen

One of the most important methods for skin cancer protection is the application of sunscreen. Sunscreen uses inorganic particles to reflect and scatter UV waves and organic particles absorb and release UV rays in the form of heat [25]. Currently, FDA recommend consumers use broad-spectrum sunscreens with SPF 15 or greater [2]. However, there are concerns regarding sunscreen ingredients that can be absorbed through the skin to the bloodstream. New FDA regulations that recommend additional safety testing for the following commonly used ingredients in the U.S.: ensulizole, octisalate, homosalate, octocrylene, octinoxate, oxybenzone, and avobenzone [26]. These active ingredients have the potential to mimic hormones or cause skin allergies, and testing is needed to confirm they do not cause endocrine disruption, cancer, or other health harms [27].

2.4 Ultraviolet Light

Ultraviolet light is wave within the region in the electromagnetic spectrum with a wavelength between 400 to 10 nanometers [28]. In this spectrum, UV radiation has enough energy to cause ionization that breaks electrons from atoms [29]. The Sun is the source of ultraviolet radiation and can be categorized into UV-A, UV-B, and UV-C [30]. UV-C rays, 100-290nm, are the most harmful but do not pass Earth's ozone layer. About 95% of the UV-B rays, 290-320nm, are absorbed by the ozone in the stratosphere, and UV-A, 320-400nm, has the longest wavelength that reaches Earth's surface in greatest quantity [31]. UV-A has enough energy to penetrate the epidermis, dermis, and hypodermis, while UV-B can penetrate only through the epidermis and slightly into dermis [31]. Therefore, UV-A and UV-B reaches humans and increases sunburn and the risk of DNA and cellular damage; this increases the risk of skin cancer [32]. These properties of UV light allow for other applications in sterilization/disinfection, fluorescence/lighting, and curing [33].

2.5 Cell Anatomy

The human body is made up of eukaryotic cells that contain a cell membrane, cytoplasm, and organelles. The cell membrane acts as a barrier that regulates incoming/outgoing materials that is made up of two phospholipids with their hydrophilic heads facing outward and hydrophobic tails facing each other called a phospholipid bilayer [9]. The cytoplasm is a watery interior that houses ions, proteins, and organelles that are responsible for hemostasis [9].

Organelles perform specialized tasks and work symbiotically to allow for differentiation among cells. Some of the most important organelles are highlighted in

Figure 1. Protein rich organelles such as intermediate filaments, microtubules, and microfilaments provide structural integrity and allow movement [9]. The ribosomes attached to endoplasmic reticulum and free-floating ribosomes are responsible for protein production [9]. The golgi apparatus processes proteins and packages them in vesicles called lysosomes [9]. Mitochondria generate energy for the cell [9]. Lastly, the nucleus contains the cell's DNA which carry the instruction for all processes [9]. The nucleus is surrounded by a nuclear membrane that limits entering and exiting similar to the cell membrane [9].

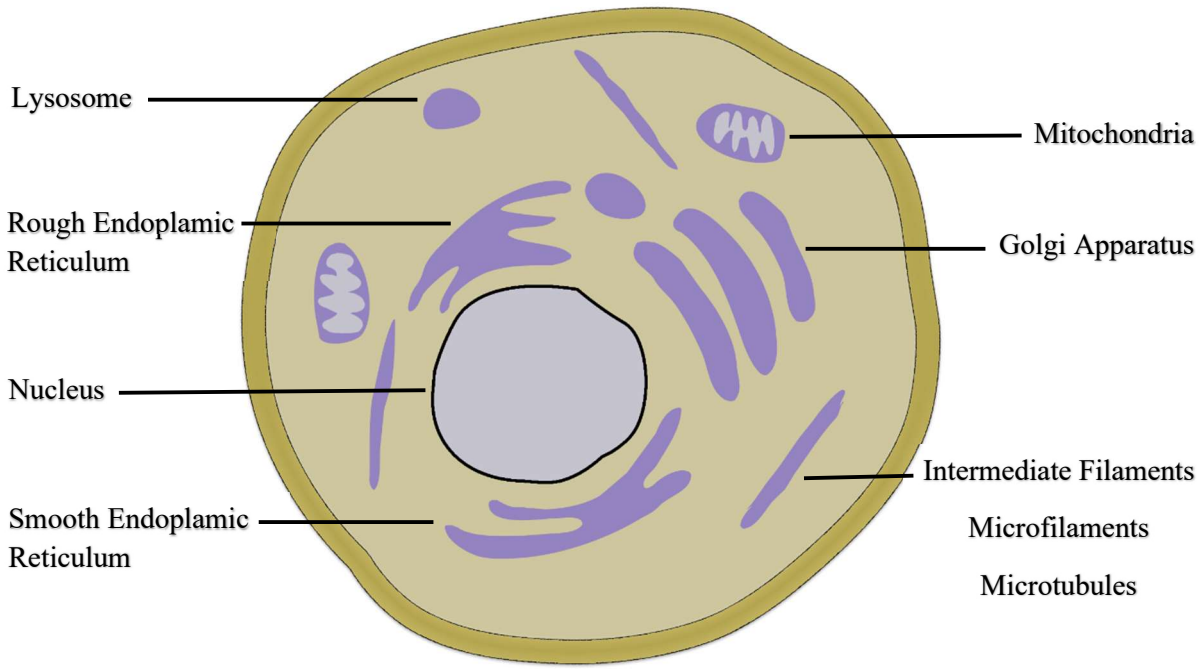

Figure 1: Cell Anatomy.

2.6 DNA Damage

UV light can directly and indirectly cause DNA damage. A photon of UV light can directly activate the DNA by fusing two pyrimidine base pairs together and causing difficulty in replication [34]. It can also damage the DNA indirectly by causing melanin

to react an adjacent oxygen atom and forming a reactive species [34]. Activated oxygen reactive species can interact with the DNA to replace purine guanine to pyrimidine thymine and cause incorrect transcription [34]. Furthermore, activated oxygen can also interact with hydrogen and form two hydroxyl radicals that attach to the DNA's backbone (deoxyribose) and break the strand or release a base pair [34]. Defense mechanisms such as nucleotide excision repair, base excision repair, and increased melanin production all try to combat UV damage [34].

2.7 P21

Cyclin kinase inhibitors (CKIs) are proteins that bind to cyclin and prevent the phosphorylation activities of cyclin-dependent kinases (CDKs) [35]. The main function of CDKs is to promote transcription and mitosis; CKIs work to prevent these processes [36]. CKIs are important tools in controlling proliferation of cells that have experienced damage or mutations [36]. P21 is one type of cyclin-dependent kinase inhibitor that affects the following mechanisms: cell cycle, DNA replication/repair, and apoptosis [37].

During the cell cycle, CDKs are activated by pairing with specific cyclins corresponding to different checkpoints for cell replication [38]. During one of these phases, p21 inhibits progression of the cell cycle by binding G_1/S-phase and S-phase CDKs and blocking cell from entering S phase [37]. Proliferating cell nuclear antigens (PCNAs) are responsible for DNA replication and/or repair [39]. P21 inhibits DNA replication by binding to PCNAs rendering them unable to activate DNA polymerase [39]. Lastly, p21 has been observed to be cleaved by caspase 3, a protease enzyme responsible for DNA fragmentation, which causes abnormal cell apoptosis [40]. These mechanisms promote cell cycle inhibition, but surprisingly, protects the cell from

immediate apoptosis because an active cell cycle is needed to trigger apoptosis [7]. Therefore, p21 detection was used as the metric for measure cell damage due to UV irradiation.

2.8 Sphingomyelin

Sphingomyelin (SM) is prevalent in many mammalian cells and tissues and some major functions include creating lateral structures (e.g. Lipid rafts) and interacting with membrane-spanning proteins and cell signaling events [4]. SM is composed of long-chain bases, fatty acids, and a glycerol-based backbone [4].

2.8.1 Lipid Rafts

Within the fluid bilayer, SM and cholesterol form lipid rafts that are tightly packed due to the hydrophobic nature of their saturated fatty acid side chains [41]. Cytoplasmic proteins attach to these rafts by covalently bonding to the saturated fatty acids and cell surface proteins attach via glycosylphosphatidylinositol [41]. Glycosylphosphatidylinositol is a lipid anchor that covalently attaches to the carboxyl terminus of cell surface proteins [42]. Lipid rafts are especially important in trafficking proteins from the Golgi complex to the cell surface and vice versa because they ensure specificity and fidelity [43].

2.8.2 Signaling Pathways

Sphingomyelin is involved in many signaling pathways, one being its role in apoptosis. The sphingolipid ceramide pathway is hypothesized to be the key regulator of programmed cell death. This pathway involves sphingomyelin using the enzyme sphingomyelin synthase to form ceramide and phosphorylcholine [44]. Ceramide is a neutral, lipid molecule composed of long-chain sphingoid base, sphingosine, and a

variety of acyl groups [45]. Ceramide then works to activate nuclear factor kappa light chain enhancer of activated B cells (NF-κB) [46]. The primary function of NF-κB is the transcription of genes that activate cell apoptosis [47].

2.8.3 Bovine Sphingomyelin

Bovine sphingomyelin (BSM) was selected because it is found in common foods, such as dairy products, eggs, and soybeans, and it has a consistent molecular structure [48]. Its uniformity in molecular structure may be due to the cows' consistent, controllable diet [48]. Figure 2 shows the chemical structure of BSM; its composed of sphingosine, fatty acid residue, and phosphocholine group [49]. It has a molecular weight of approximately 785 g/mol that slightly fluctuates based on the fatty acid distribution, and it was obtained in powder form [49].

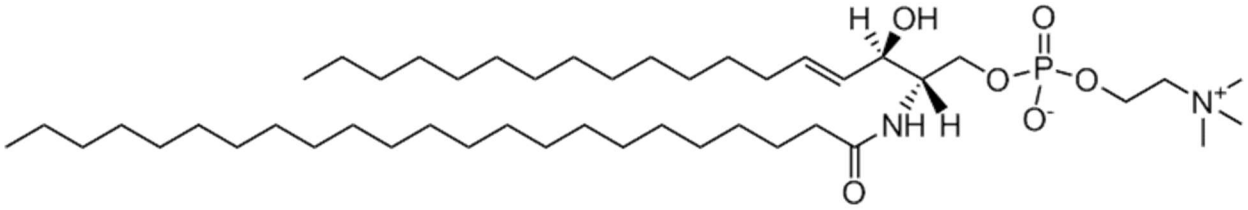

Figure 2: Bovine Sphingomyelin. Representative structure of one of many possible structures. [49]

2.8.4 Fluorescent Sphingomyelin

Currently, BSM tracking efforts using confocal microscopy do not work because the SM is not fluorescent. Fluorescent sphingomyelin (FSM) was developed to track intracellular mechanisms. FSM differs from BSM by the introduction of a fluorescent tag marked by a red rectangle in Figure 3 [50]. Avanti Polar Lipids Inc. manufactures a specific FSM labeled C6-NBD Sphingomyelin that has a molecular weight of 741 g/mol and chemical formula of $C_{35}H_{61}N_6O_9P$ [51]. Similar to BSM, it was obtained in powder

form. However, modification was needed to suspend the FSM in light limiting conditions due to light sensitive nature of FSM.

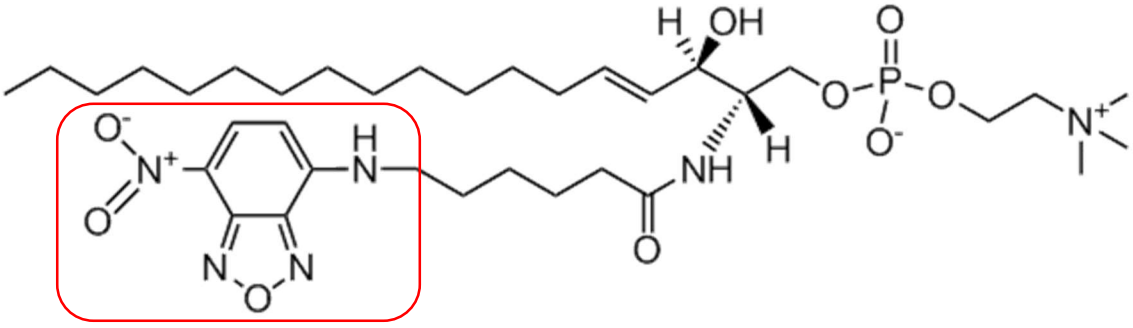

Figure 3: Fluorescent Sphingomyelin (FSM). The red rectangle marks chemical structure of the fluorescent tag. [51]

2.8.5 Dietary Sphingolipids

Recent research shows that certain dietary changes can reduce the prevalence of nonmelanoma skin cancer [52]. Sphingolipids are found in all types of foods, the most common being dairy products, eggs, and soybeans [53]. Sphingolipids in nutrition could be an avenue of skin cancer prevention [53]. Dietary sphingolipids have been studied in mice and there is a correlation between the amount of sphingomyelin fed versus amount found in the colon [54]. Consumption of sphingomyelin affects the behavior of colonic cells and inhibits the formation of colon cancer [55]. Furthermore, low doses of sphingolipids were effective in inhibiting carcinoma development [56].

Understanding the metabolism of sphingomyelin within skin cells is the first step in developing supplements or promoting certain diets that can help prevent skin cancer.

2.9 Previous Experimentation

Previous experimentation was done by California Polytechnic Bioimaging Lab to establish protocols for BSM incubation, UV irradiation, and immunostaining, found in

Appendix A. This protocol was used for preliminary testing and to confirm results previously found by Campbell [57]. Experimentation performed by Campbell suggested BSM photoprotection exists for a monolayer of keratinocytes [57].

Additionally, experimentation by Kandell determined the FSM protocol for use with keratinocytes as well as possible reduced BSM and FSM incubation time points [5]. These time points were tested using a new secondary AF 594 to determine at which time FSM and BSM shared the same photoprotective effects, Section 4.4.

Lastly, efforts made by Fraser outlined a systematic approach for image analysis [58]. With the use of macros, ImageJ produced quantitative results that eliminated possible bias if images were processed manually. Macros for data analysis are found in Appendix B.

3 METHODS

3.1 Keratinocyte Cell Culture

Human Epidermal Keratinocytes from Neonatal Foreskin (HEKn PCS-200-010, ATCC Manassas, VA) were cultured in physiological conditions (37°C, 5% CO_2) with aseptic techniques with media being replaced every two days. Media was prepared under manufacturer guidelines of combining a Keratinocytes Growth Kit (PCS-200-040, ATCC, Manassas, VA) with Dermal Cell Basal Media (PCS-200-030, ATCC, Manassas, VA) and sterile filtering the solution with a 0.22um filter. For experiments, cells were expanded in T-75 Corning Tissue Culture Flasks (BD353136, VWR, Visalia, CA) and passed into 8-well Nunc Lab-Tek Chambered Coverglasses from Thermo Scientific (43300-774, VWR, Visalia, CA). Passage number of keratinocytes for all experiments ranged between 4-5. Morphology was assessed and confluency was at least 70% before any experimentation.

3.2 Sphingomyelin Treatment

3.2.1 Bovine Sphingomyelin Solution

A 0.1% bovine sphingomyelin (BSM) solution was made by combining Bovine Milk Sphingomyelin (860063P-25mg, Avanti Polar Lipids, Alabaster, AL) and keratinocyte media solution. To determine the amount of keratinocyte media solution needed for the mixture, the number of wells was multiplied by 0.4 mL (0.4 mL*(# of Wells)). To determine the amount of BSM needed for a 1% BSM solution, that volume was then converted into grams and multiplied by 0.001 (0.4 mL*(# of Well)*(1 gram / 1 mL)*0.001 grams). These components were vortexed until homogeneous and the solution was sterilized using a 22 mL filter.

Prior to use, BSM solution was warmed in a 37°C water bath. When the keratinocytes reached a confluency of 70% or greater, the keratinocyte media solution was aspirated and 200 µL of BSM solution was dispensed to each well. Experimentation was done to analyze optimal incubation period in Section 4.4. BSM was incubated for 2 hours unless specified.

3.2.2 Fluorescent Sphingomyelin Solution

Fluorescent SM (FSM) or C6-NBD Sphingomyelin (810218P-1mg, Avanti Polar Lipids, Alabaster, AL) was dissolved in 1.35 mL of ethanol (200 proof 100%) to obtain a 1 mM stock solution. It was stored in the freezer (-20 °C) in a glass container and protected from light. In order to make 10mL of fluorescent sphingomyelin (FSM), 10mL of keratinocyte media solution, 50 µL of ethanol-FSM stock, and 3.5 mg of Bovine Serum Albumin (BSA) were combined. These components were vortexed until homogeneous and a 22 mL filter was used to sterilize the solution. The solution was then refrigerated and covered to avoid light exposure.

Prior to use, the FSM solution was warmed in a 37°C water bath. When the keratinocytes reached a confluency of 70% or greater, keratinocyte media solution was aspirated and 200 µL of FSM was dispensed to each well. Experimentation was done to analyze optimal incubation period in Section 4.4. FSM was incubated for 2 hours unless specified.

3.3 UV Treatment

UV irradiation treatment exposed strong UV radiation to skin cells that would cause cell damage or cell death. In order to maintain aseptic conditions, all equipment was sprayed with 70% Isopropyl Alcohol (IPA) before placement in the culture hood. To

calculate UV exposure time, a UV lamp (95-0251-01, UVP, LLC, Upland, CA) was placed on top of a black containment box and a UV sensor (S120UV, ThorLabs, Newton, NJ) was placed on the blue slider meant to be the treatment surface, shown in Figure 4.

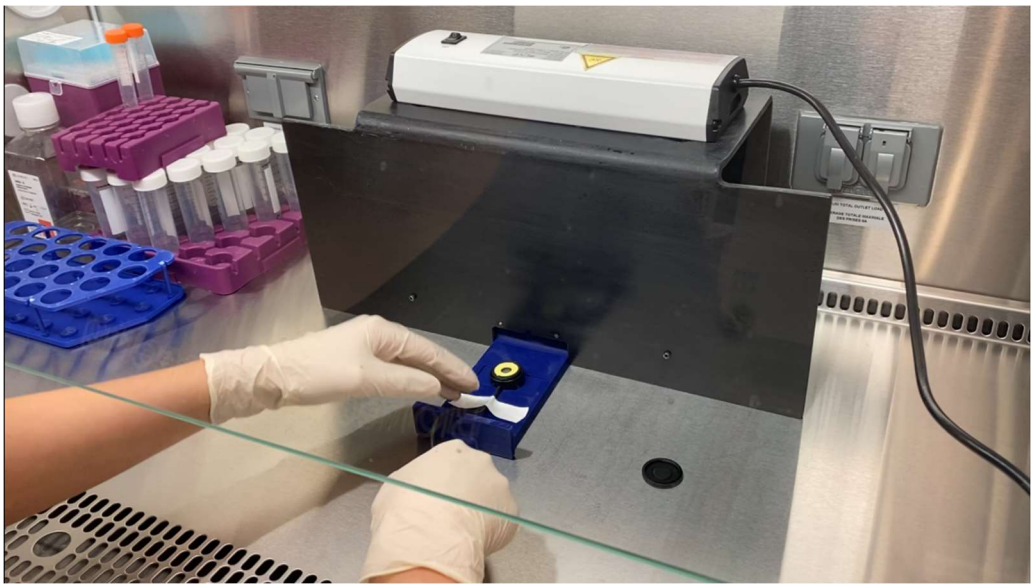

Figure 4. UV irradiation. Components included UV lamp, black containment box, blue slider as treatment surface, and UV sensor connected to power meter.

Initially, calibration was needed to determine the strength of the UV lamp on the treatment surface. After approximately 5 minutes of the UV lamp being turned on, the UV sensor was placed on the treatment surface and the power meter (PM100, ThorLabs, Newton, NJ), connected to the sensor, outputted the average power intensity in μW. The power was divided by the sensor area of 0.7088cm^2 to get the average measured irradiance of the UV lamp. Optimal UV irradiation was determined from previous lab experimentation to be 40 mJ/cm^2, Section 2.9. In order to administer this amount, exposure time was determined using Equation 1.

$$Exposure\ Time\ (seconds) = \frac{Optimal\ UV\ Irradiation\left(\frac{mJ}{cm^2}\right)}{\left(\frac{1mW}{1000\mu W}\right) * Measured\ Irradiance\left(\frac{\mu W}{cm^2}\right)} \quad \text{(Equation 1)}$$

Exposure time was typically 90 seconds. After exposure time was determined, the plate's media was aspirated and new keratinocyte media solution was dispensed. The plate's top covering was removed and the plate was placed on the treatment surface for the calculated exposure time. Treatment was applied to all wells in a plate and no modifications of the plates were done to try to differ UV treatments within each plate. After UV irradiation, plates were stored in an incubator for an additional 24 hours before being fixed.

3.4 Fixed Cells for Immunostaining

Fixation preserves biologics from decay due to autolysis or putrefaction. It stops ongoing cellular mechanisms and increases their stability [59]. The three steps for cell fixation are fixation, permeabilization, and blocking.

Figure 5 is a visual representation of the steps of cell fixation. In Figure 5A, fixation stops cellular mechanisms and turns cells from dynamic to static. In Figure 5B, permeabilization introduces gaps in the lipid membrane of the outer wall and nucleus. In

Figure 5C, blocking prevents binding of non-target molecules such as the organelles in the cell.

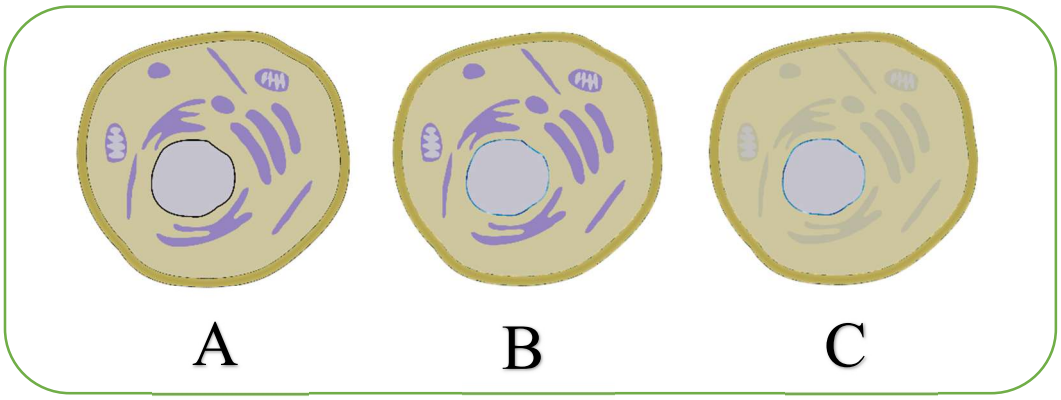

Figure 5: Steps of Cell Fixation. A. Fixation, cross-links plasters cell into a static state B. Permeabilization, creates gaps within the cell membrane and nucleus C. Blocking, reduces interaction with non-target molecules.

3.4.1 Fixation

Cells were fixed prior to immunostaining to allow antibodies to access intracellular structures. Fixation using paraformaldehyde caused covalent cross-links between molecules and plastered them together while they would otherwise fall apart and diffuse away [60].

Paraformaldehyde 16% (EM Grade 15710, Electron Microscopy Sciences) was combined with 1% Phosphate Buffered Solution (PBS) to create paraformaldehyde 3.7% (PFA). Twenty-four hours after UV irradiation, the media was removed from wells and one wash was performed with PBS. PBS was then removed, and wells were fixed with 200 µL of PFA. Plates were incubated for 15 minutes while minimizing light exposure. After allotted time, wells were washed three time with PBS.

3.4.2 Permeabilization

Permeabilization breaks and removes cellular membrane lipids to allow large molecules such as antibodies to enter a cell and its nucleus. Triton X-100 was combined with 1% PBS to create 0.1 %Triton X-100 solution. After fixation, plates were incubated for 20 minutes with 200 µL of Triton X-100 and three more washes of PBS were gently applied.

3.4.3 Blocking

Blocking is important to reduce the amount of interaction between the immunostaining antibodies and non-target molecules called non-specific binding. This reduced nonspecific "background" staining and increased signal to noise ratio [61]. Normal Goat Serum 10% (500622, Life Technologies) was combined with 1% PBS to create 1% blocking solution. After permeabilization, plates were incubated approximately for 12 hours at 4°C with 200 µL of blocking solution. Three more washes of PBS were done prior to immunostaining.

Fixation, permeabilization, and blocking steps for experiments were outlined above. Table 1 summarizes concentrations, incubation times, and materials for each of these steps.

Table 1: Cell Fixation.

Procedure	Concentration	Incubation Time	Materials	Manufacturer
Fixation	3.7%	15 minutes	Paraformaldehyde PBS	Electron Microscopy Sciences
Permeabilization	0.1%	20 minutes	Triton X-100 PBS	Invitrogen HFH10

Blocking	1%	~12 hours	Normal Goat Serum PBS	Life Technologies

3.5 Immunostaining

Dual labeling is a staining method that uses two antibodies to target a specific antigen and to allow for immunofluorescent tagging. P21 is the protein of interest and the indirect immunostaining protocol was previously optimized by the lab, Section 2.9. Figure 6 is a visual representation of immunostaining of a cell. In Figure 6A, indirect immunostaining targeted p21 to appear green under a certain emission spectrum. Further staining of the cell's nuclei under a different emission spectrum was done to quantify cell count in Figure 6B.

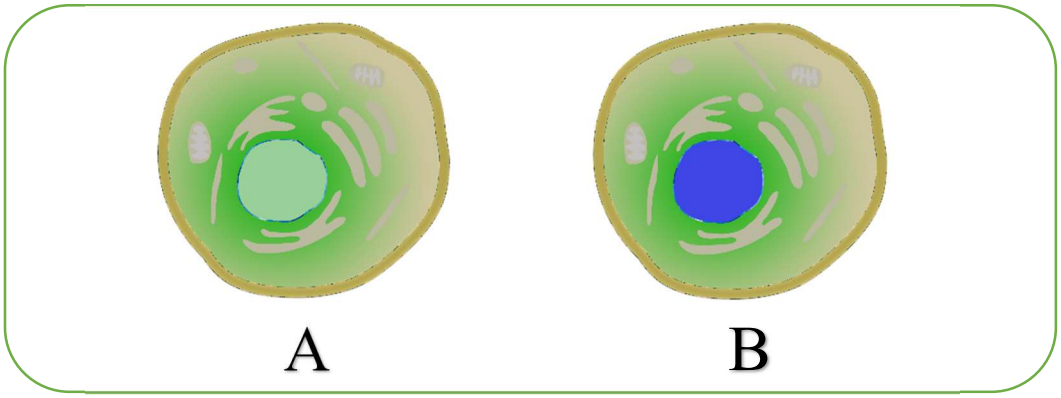

Figure 6: Immunostaining of Cell. A. Indirect immunostaining allows fluorescence of p21. B. Hoechst allows fluorescence of cell's nucleus.

A closer observation of indirect immunostaining is found in Figure 7. Figure 7A represents the target molecule, in this case, it is p21. In Figure 7B, the primary antibody has specific receptors that attaches to antigen. Lastly in Figure 7C, secondary antibodies

have specific receptors that attach to that primary antibody. These secondary antibodies have fluorescent tags that emit light under a specific range frequency.

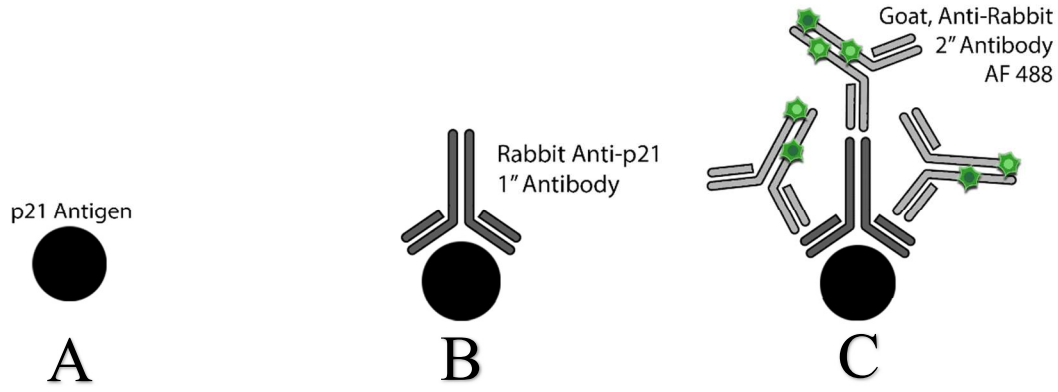

Figure 7: Indirect immunostaining. A. Target molecule B. Primary binds to that specific antigen C. Secondary with fluorescent tag binds to primary. The signal/intensity is amplified because more than one secondary can bind a primary.

3.5.1 Primary

The primary antibody binds to the specific p21 antigen. Following blocking, plates were incubated with a primary antibody. Anti-p21 antibody rabbit (Abcam ab18209) was combined with 1% PBS to create 1:400 p21 antibody. Plates were incubated for 9 hours at 4°C with 200 µL of p21 antibody. The primary was then washed off gently 3 times with PBS.

3.5.2 Secondary

The secondary antibody binds to the heavy chains of primary antibody that do not interfere with primary antibody's binding to antigen [62]. Two secondary antibodies, carrying different-colored fluorophores, were used to visualize p21 concentration within the cell. Two secondaries were needed because FSM shared the same emission spectrum as the initial secondary. Figure 8A/8B illustrates treatments of no sphingomyelin and

BSM using the first primary, AF 488 goat, anti-rabbit IgG (ThermoFisher Scientific A-11008). In Figure 8C, the clarity of p21 presence was lost because FSM shares the same emission spectrum and would add to its intensity. In order to mitigate this, a new secondary, AF 594 goat, anti-rabbit IgG (ThermoFisher Scientific A11037), with a different emission spectrum was introduced to separately quantify FSM and p21, Figure 8D.

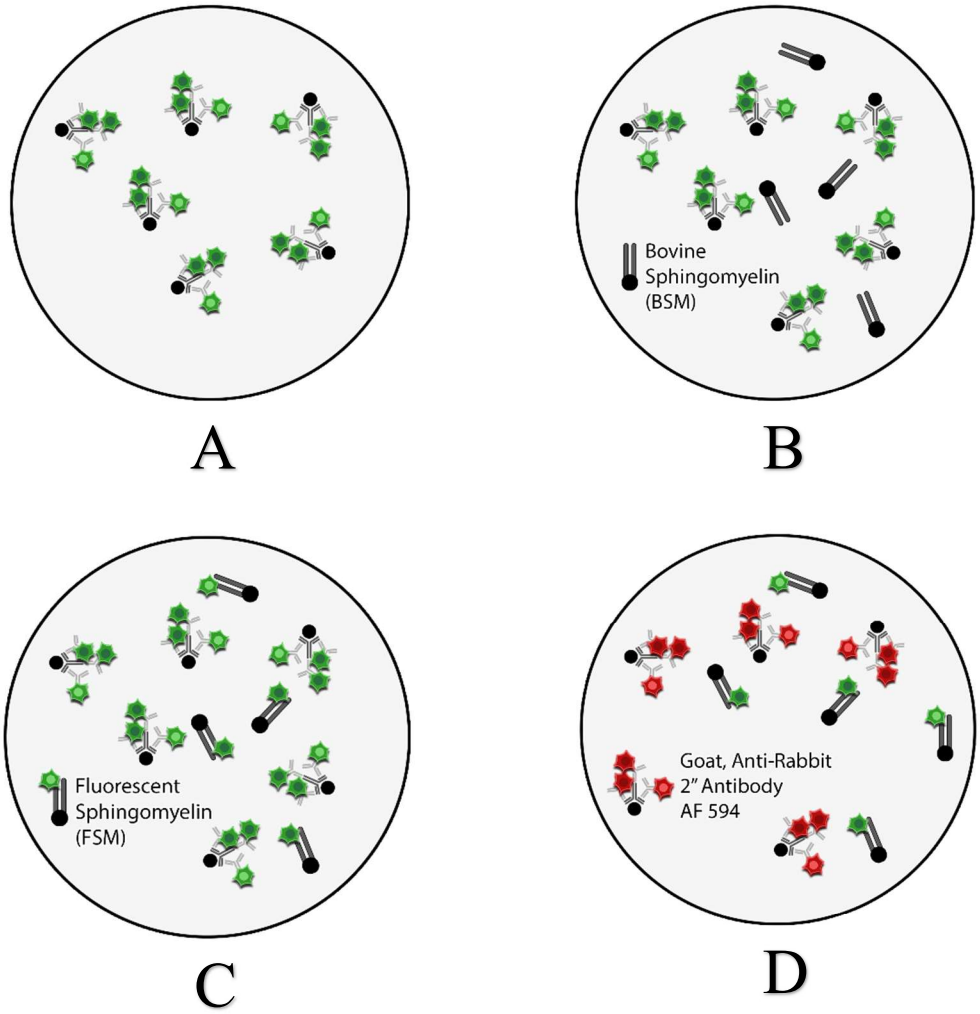

Figure 8: Fluorescence Emission for Different Secondaries. A. p21 stained with Secondary AF 488. B. p21 stained with Secondary AF 488 with the introduction of BSM.

C. p21 stained with Secondary AF 488 with the addition of FSM. They fluoresce the same color because they share the same emission spectrum. D. p21 stained with Secondary AF 594. FSM fluoresces green while p21 fluoresces red.

AF 488 goat, anti-rabbit IgG was combined with 1% PBS to create 1:400 AF 488 secondary. Experimentation with AF 594 goat, anti-rabbit IgG) and 1% PBS was summarized in Section 4.3 in order to optimize fluorescence using a 1:200 AF 594 secondary. Following primary, plates were incubated for 1 hour with 200 µL of either AF 488 or AF 594 secondary. The secondary was then washed off gently 3 times with PBS.

3.5.3 Nuclear Staining

Lastly, nuclear staining was introduced to help focus cells during confocal microscopy, check their viability qualitatively, and obtain a cell count to help normalize intensities between UV and non-UV cases. Hoechst 34580 (Life Technologies H21486) binds to all nucleic acids and has a blue fluorescent excitation and emission. Hoechst 34580 was combined with 1% PBS to create 0.015% Hoechst stain after reduction of 0.03% Hoechst was deemed equivalent, from experimentation found in Section 4.3. Following secondary, plates were incubated for 15 minutes with 200 µL of Hoechst stain. The Hoechst stain was then washed off gently 3 times with PBS. This concluded the immunostaining procedure. PBS was added to each well, plates were wrapped in foil to limit light exposure, and confocal imaging was done soon after immunostaining.

Primary, secondary, and nuclear staining steps for experiments were outlined above. Table 2 summarizes concentrations, incubation times, and materials for each of these steps.

Table 2: Immunostaining.

Procedure	Concentration	Incubation Time	Materials	Manufacturer
Primary	1:400	9 hours	Anti-p21 antibody rabbit PBS	Abcam
Secondary	1:200 (refer to Section 4.3) 1:400	1 hour	AF 594 goat, anti-rabbit IgG AF 488 goat, anti-rabbit IgG PBS	ThermoFisher Scientific
Nuclear Staining	0.015% (refer to Section 4.3)	15 minutes	Hoechst 34580	Life Technologies

3.6 Confocal Imaging

Olympus FluoView FV1000 is a confocal laser scanning biological microscope that allows for fluorescent imaging. The FluoView desktop software allows capture of multiple laser channels when captured sequentially. The following laser channels were used: DAPI for Hoechst, 488 laser for Alexa Fluor 488, and 594 laser for Alexa Fluor 594. The 20X objective was used to ensure equal cell distribution, 40X oil objective for p21 positive analysis, and 100x oil objective for FSM localization analysis. Images were saved in Olympus Image Binary format (.oib) with a size of 512x512, 16-bit, and 512K.

Three images in the center of each well were taken to avoid unequal distribution of UV that came when cells were closer to the edge of the well. High voltage (HV) and laser power were optimized for treatment for every experiment. HV is attenuation of voltages to increase signal, but if too high, it can also create visible noise [63]. Laser power refers to the percentage reduction of light using filters such as neutral density filters [63]. The settings for each experiment are summarized in Table 3.

Table 3: Optimized Laser Settings per Stain.

Experiment	Stain	High Voltage (HV)	Laser Power
1: Section 4.1	DAPI	700	1.5%
	AF 488	700	19%
2: Section 4.2	DAPI	700	1.5%
	AF 488	700	5% (FSM Treatment) 19% (BSM Treatment)
	AF 594	900	15%
3: Section 4.3	DAPI	700	1.5%
	AF 594	700	18%
4: Section 4.4	DAPI	700	1.5%
	AF 488	700	3%
	AF 594	700	18%
5: Section 4.5	DAPI	700	1.5%
	AF 488	700	6% (FSM Treatment) 15% (BSM Treatment)
	AF 594	700	18%
6: Section 4.6	DAPI	700	2%
	AF 488	700	10%

Figure 9 captures the confocal microscope's user interface and outlines location of settings for the different channels. The dashed, red rectangle highlights where the user changes the HV and the solid, red rectangle is where the user changes laser power.

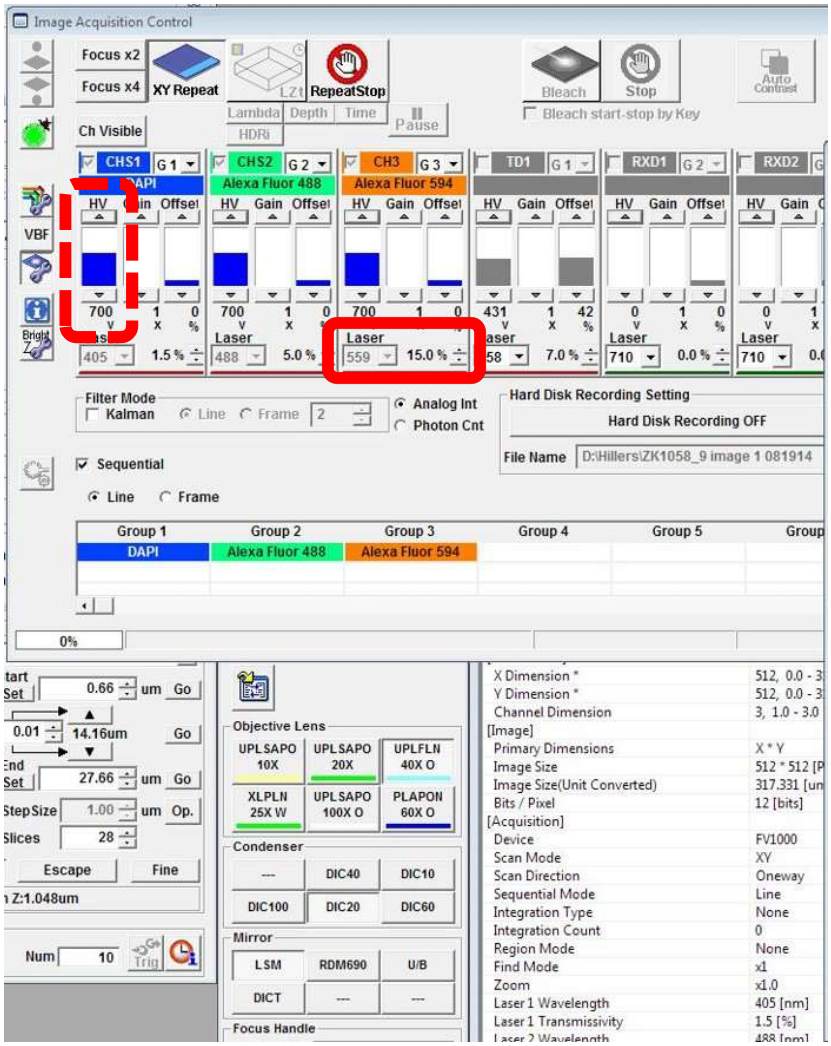

Figure 9: Image of FluoView FV1000 User Interface. The dashed, red rectangle is where user adjusts High Voltage. The solid, red rectangle is where user adjusts Laser percentage.

3.7 Image Analysis

ImageJ is an open-source, Java-based program that provides quick, automated image processing ideal for cell analysis. After confocal imaging, the images in .oib format were opened in ImageJ, color channels were separated, and macros ran a series of functions to quantitatively measure images. A macro is a file that contains a series of steps that execute automatically once specific inputs are given [64]. Appendix B shows the macros used in experiments.

A variety of quantitative measurements were performed on the images, summarized in Table 4. The types of measurements were related to either the nucleus or the image intensity. Nuclei viability directly correlates with cell health; measurements such as area, shape descriptors, skewness, fit ellipse, and perimeter were taken for each nucleus to understand how nuclei behave pre and post UV irradiation. Image intensity tried to quantify how much p21 was present in the overall image to indicate how much cell damage occurred. Measurements such as mean gray value, min/max value, integrated density, mode, and median outputted quantitative values for the p21 channel. Significance was tested for each measurement to determine the important parameters that were influenced by treatments was performed in Section 4.1.

Table 4: Quantitative Measurements Available on ImageJ

Measurement	**Description**
Area	Measures area of selection in square pixels
Shape Descriptors:	
Circ. (circularity)	4π*area/perimeter^2 Output ranges from 0 (elongated shape) to 1 (perfect circle)
AR (aspect ratio)	major_axis/minor_axis Ratio of cell's size in specified dimensions
Round (roundness)	4*area/(π*major_axis^2) Inverse of the aspect ratio
Solidity	area/convex area
Skewness	Coefficient of skewness (symmetry) in x and y = 0 symmetric < 0 asymmetric to the left (tail extends left of center of mass) > 0 asymmetric to the right (tail extends right of center of mass)
Centroid	Average of all x and y coordinates to get center point of selection
Perimeter	Length of outside boundary of selection
Fit Ellipse	Finds best fitting ellipse of selection
Mean Gray Value	Sum of the gray values of all the pixels in the selection divided by the number of pixels
Standard Deviation	Standard deviation of the gray values used to generate the mean gray value
Min and Max Gray Value	Minimum and maximum gray values within the selection
Integrated Density:	

IntDen	Product of Area and Mean Gray Value
RawIntDen	Sum of the values of the pixels in the image
Modal Gray Value	Most frequently occurring gray value in the image
Median	The median value of the pixels in the image

[65]

3.7.1 Cell Count

The main reason for staining for nuclei was to obtain an accurate cell count. During UV irradiation, cells were killed and this reduced the number of cells per well. Because intensity measurement was taken per image, cell count was used to help normalize results between pre and post UV. Appendix B outlines the macro used for this analysis.

Cell nuclei were used for cell count measurement because they tended to maintain a more circular structure than cells' outer lipid bilayer. The program was able to isolate for circular structures and count how many were present per image. Initial optimization was required to establish a minimum radius to be considered a nucleus. Figure 10A shows how images from the DAPI channel were made binary and Figure 10B shows the cell count without a minimum radius. Small effects in noise were considered nuclei and greatly overestimated the number of cells present. Figure 10C shows the implementation of a minimum radius of 90 pixels in order to reduce the effect of noise and increase the level of accuracy.

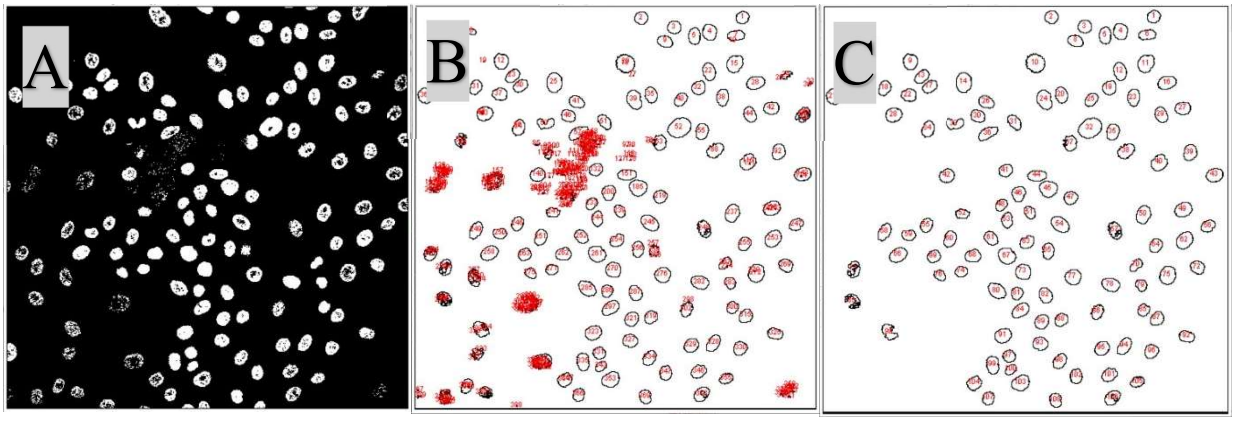

Figure 10: Cell Count Image Processing. A. Binary conversion of DAPI channel B. Cell count without minimum pixel radius C. Cell count with minimum pixel radius of 90.

3.7.2 Image Intensity

To study the amount of cell damage due to UV irradiation, p21 intensity was measured. Presence of p21 is directly proportional to an increase in cell damage and differences in intensity support the effectiveness of sphingomyelin against UV irradiation. P21 intensities were taken per image and mean, min, max, median, and mode were initially analyzed for significant differences, Section 4.1. The use of two secondaries were used based on the treatment given (i.e. BSM v. FSM) explained in Figure 8. Therefore, images were separated based on their secondary treatment and comparisons were limited to wells sharing the same secondary type. Appendix B outlines the macro used for this analysis.

3.7.3 Nested Values

A nested design or hierarchical design is when a factor is a subset of another. In a nested design, each observation has a unique identity because it has a specific factor not replicated across each treatment [66]. Current experimentation methods yield a 2-level nested design where each observation is unique because its location among the 8 wells and its overall plate is not consistent per treatment, shown in Figure 11.

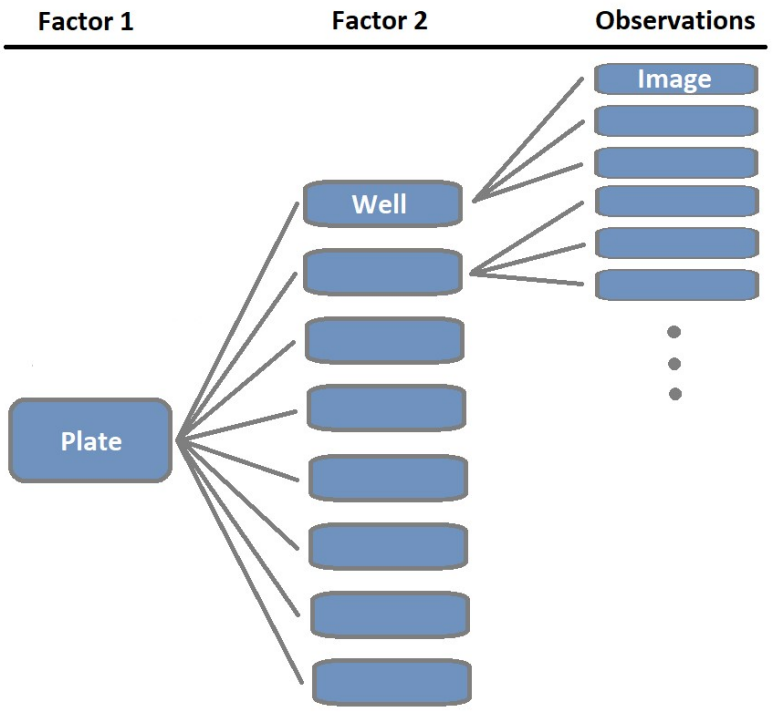

Figure 11: Nested Factors. Each Image has a factor of Well, and each Well has a factor of Plate.

A linear model can be used to explain this nest design where the response variable is affected by the treatment as well as the variability from each factor, Equation 2.

$$y_{abc} = \mu + \alpha_a + \beta_{b(a)} + \varepsilon_{abc} \qquad \text{(Equation 2) [67]}$$

where

y_{abc}	response variable
μ	overall mean
α_a	effect of factor Plate
$\beta_{b(a)}$	effect of factor Well within each level of Plate
ε_{abc}	unexplained variation (error term) – variation within each Image

There is a significant effect of p21 intensity results due to the Well and due to the Plate. In order to negate these effects, values were averaged per plate and sample size

was determined by number of plates. This greatly reduced the number of samples, however, it allowed analysis of effects of treatments rather than effects due to nested factors.

3.7.4 Gaussian Blur

Gaussian blur is a way to apply a low-pass blurring filter to an image in order to reduce noise and detail. The Gaussian function creates new image by taking a weighted average with the colors near the pixel of interest having more weight than those farther away. This removes or smooths rapid changes in pixel intensity and reduces the number of "outlier" pixels that can cause noise [68].

A Gaussian Blur plugin was installed to ImageJ for image processing [69]. The gaussian blur was applied to images in order to observe FSM localization, Section 4.5. In Figure 12A, a line of interest was made across a cell to determine its intensity and Figure 12B shows its profile plot without filtering. A clearer intensity profile was observed after applying Gaussian Blur, Figure 12C. This was because the overall intensity was captured without the noise of the pixels. It was concluded gaussian blur was an appropriate filtering method prior to analyzing FSM location within a cell.

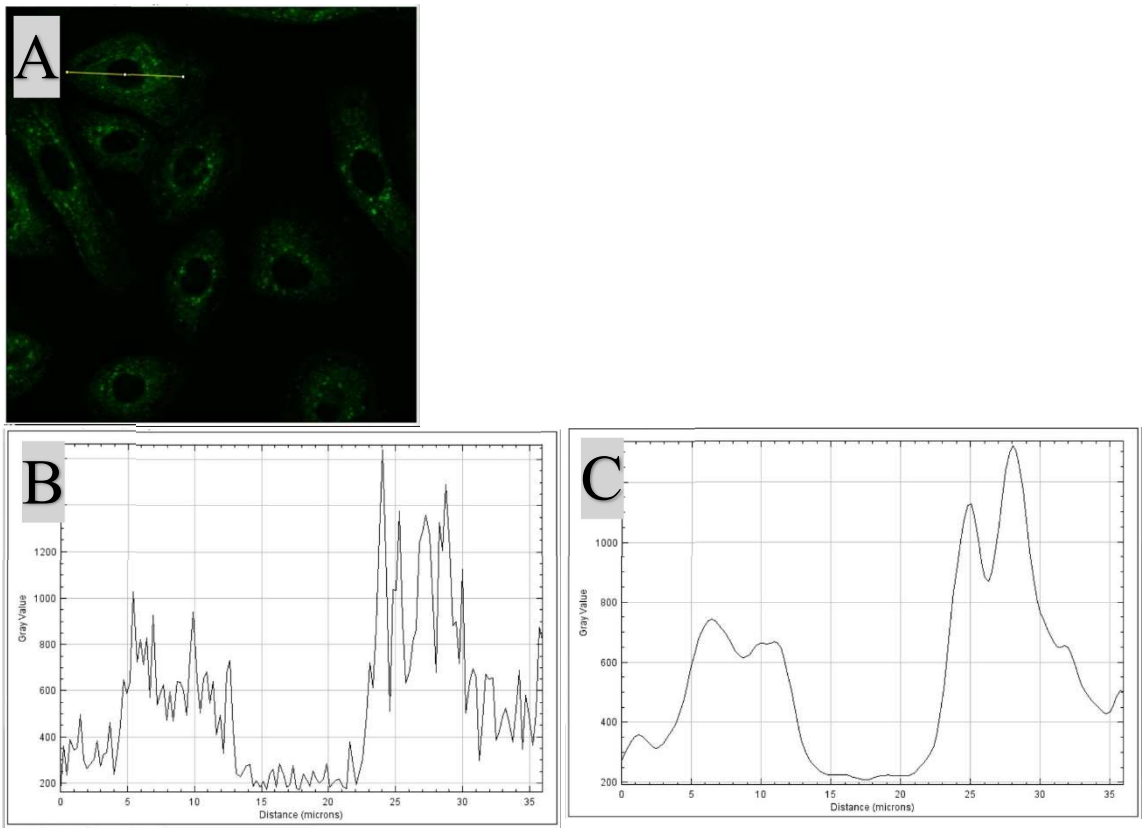

Figure 12: Gaussian Blur. A. FSM Channel with the line of interest for profile plot across the diameter of cell. B. Profile plot without filtering. C. Profile plot with Gaussian Blur filter.

4 SUMMARY OF EXPERIMENTS

Table 5: Summary of Experiments.

Experiment	Goal	Thesis Section
1. Replication of Previous Experimentation	1: Replicate procedure and compare results. 2: Identify new parameters that introduces variation between treatments.	Section 4.1
2. FSM Treatment	1: Replicate FSM procedure 2: Introduce new Secondary AF 594	Section 4.2
3. Optimizing New Secondary Concentration	1: Optimize for new Secondary AF 594 2: Evaluate reduction of Hoechst concentration	Section 4.3
4. Optimizing Incubation Time	1: Optimize FSM incubation with new Secondary AF 594 concentration	Section 4.4
5. FSM Localization	1: Compare FSM with BSM 2: Observe the distribution of FSM within keratinocytes	Section 4.5
6. Experiment replication with updated protocol	1: Replicate previous experimentation results using new substrates, materials, and slightly modified procedure 2: Understand variation between experiments	Section 4.6
7. Compiled data analysis	1: Understand inter and intra subject variation 2: Evaluate treatment effects on new parameters and its significance 3: Estimate number of trials needed for statistical significance	Section 4.7

4.1 Replication of Previous Experimentation

4.1.1 Objectives/Methods

The main purpose for this experiment was to replicate results using the protocol created by previous lab's experimentation. Previous lab experiments found the optimal procedure for UV treatment, staining, and analysis, Section 2.9. This procedure was documented in Appendix A and replication efforts were needed to confirm results and identify new parameters of interest.

Goal 1: Replicate procedure and compare results.

Replication of previous experiments ensures results are valid and that protocol is immune to external variation. Some key sources of external variation include handling techniques of the engineer performing experiment and specific batch of reagents used. This experiment documents that these sources of variation were minimized, and results were compared to previous experiments.

Goal 2: Identify new parameters that introduces variation between treatments.

Treatments, staining, and confocal imaging remained unchanged for this experiment, however, investigation of ImageJ image processing software showed additional quantitative functions that could be applied to the images summarized in Section 3.7. New parameters were tested for significance in the hopes that they would further explain the variation between treatments.

Experimental procedure was not modified from protocol established by previous lab experiments, Appendix A. Lab culturist seeded 8, 8-well plates and incubated/feed plates until the center of each well had a confluency greater than 70%. There were 2

explanatory factors, SM and UV, that were crossed to produce 4 different treatments distributed to 2 plates each, Figure 13. The different treatments were No SM + No UV, BSM + No UV, No SM + UV, and BSM + UV.

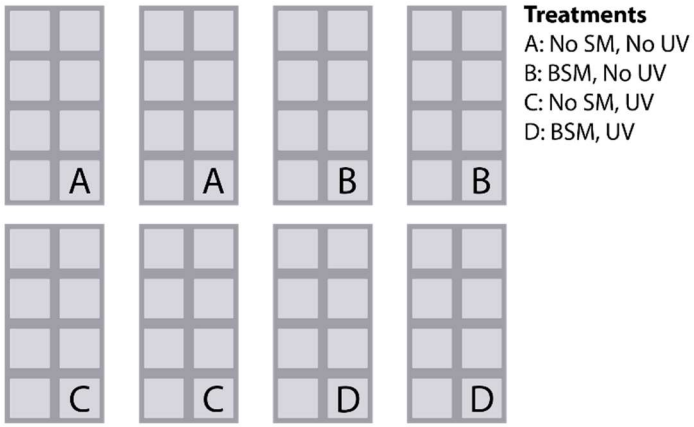

Figure 13: Design of Experiment 1. There was a total of 8 plates. There were 4 treatments with 2 plates receiving each treatment.

4.1.2 Results

For this experiment, the lab protocol, shown in Appendix A, was replicated. Success of immunostaining was observed to be qualitatively appropriate. In Figure 14A, the DAPI channel had distinct globular outlines assumed to be cells' nuclei. In Figure 14B, the AF 488 channel had some high fluorescence areas corresponding to the globular outline in the DAPI channel. This indicates that there was p21 damage markers caused presumably by the UV irradiation.

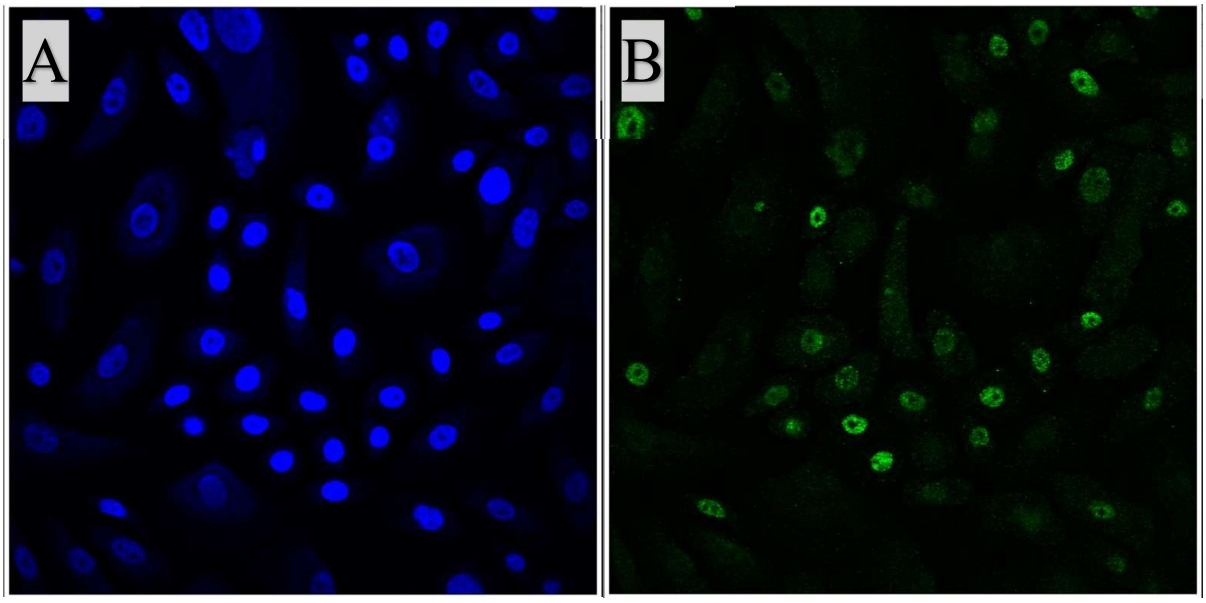

Figure 14: Experiment 1 Confocal Imaging. A. DAPI Channel displaying cell nuclei. B. AF 488 channel displaying p21 indirect immunostaining.

Images were then quantitatively assessed using ImageJ. The cell count macro was used on the DAPI channel and the intensity macro applied on the AF 488 channel, found in Appendix B. Additionally, new parameters were also evaluated for the shape of cell nuclei and for intensity measurements such as min and max, summarized in Table 4. Because each well was tied to their specific plate, nested techniques were used the find the average of the values per plate, Section 3.7.3. Statistical analysis lacked power because sample size for each treatment was 2, but observing trends was sufficient for this experiment.

Cell count was first analyzed to understand how many were killed during UV treatment. UV irradiation was effective in producing cell death shown by a significant decrease in cell count between UV and non-UV treated plates, Figure 15. Plates treated with BSM had an average of 45 cells per image before UV irradiation and an average of 29 cells per image post. Plates treated with no sphingomyelin had an average of 67 cells

per image before UV irradiation and an average of 28 cells per image post. Variation in cell count between No SM + No UV and BSM + No UV may be due to a combination of plate variation and an enlargement of cells due to BSM addition.

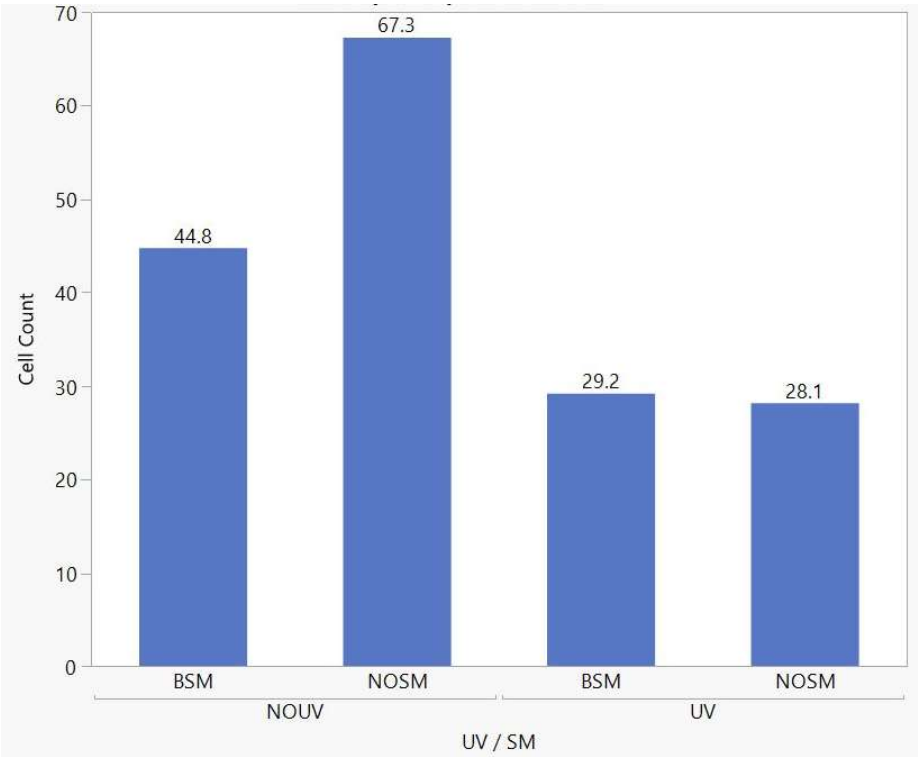

Figure 15: Experiment 1 Cell Count (n=8).

In order to analyze the difference of p21 concentrations between treatments, plates were normalized by dividing intensity with cell count. Figure 16 shows treatment No SM + UV to have the highest concentration of the p21 positive cells indicating the most cell damage. Treatment BSM + UV had a reduced the p21 concentration compared to No SM + UV. These results were similar to previous experimentation [57].

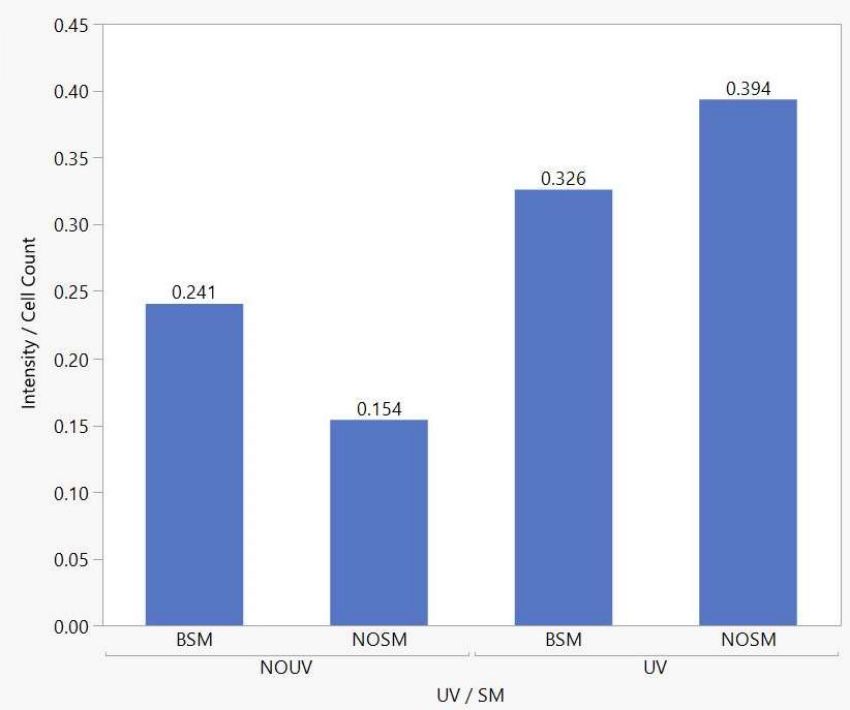

Figure 16: Experiment 1 p21 Intensity (n=8).

JMP is a powerful statistical software that can fit multiple models against full-factorial explanatory variables. ANOVA was done with all quantitative measurements available on ImageJ listed in Table 4. These additional parameters were treated as independent response variables in the hopes of identifying new metrics that explain variability between treatments, Figure 17.

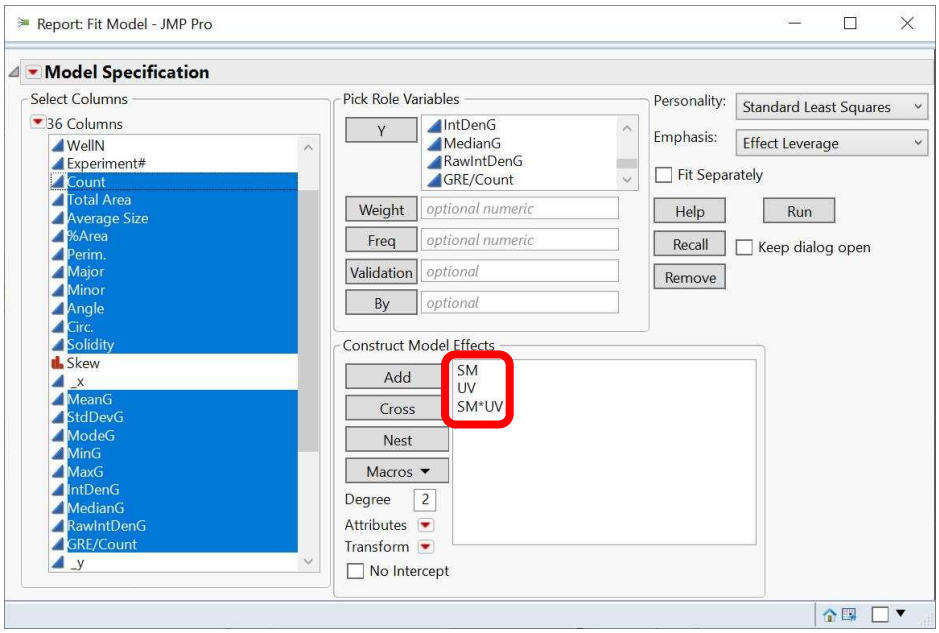

Figure 17: Image of JMP Fit Model User Interface. The section highlighted blue are all the response variables tested. The red box shows all the explanatory variables; SM*UV evaluates how the interaction between treatments effects results.

The parameters that showed significant difference between treatments aside from cell count and intensity, were min/max values and nucleus circularity. A logarithmic scale shows the mean minimum and maximum intensities from AF 488 images, Figure 18. Minimum values correspond to dark areas in an image where no cells are present. Maximum values correspond to the highest areas p21 aggregated within a cell. This metric could serve as a gateway check to filter results that are abnormal. Based Experiment 1 results, minimum value should be less than 1 and maximum value should be 255.

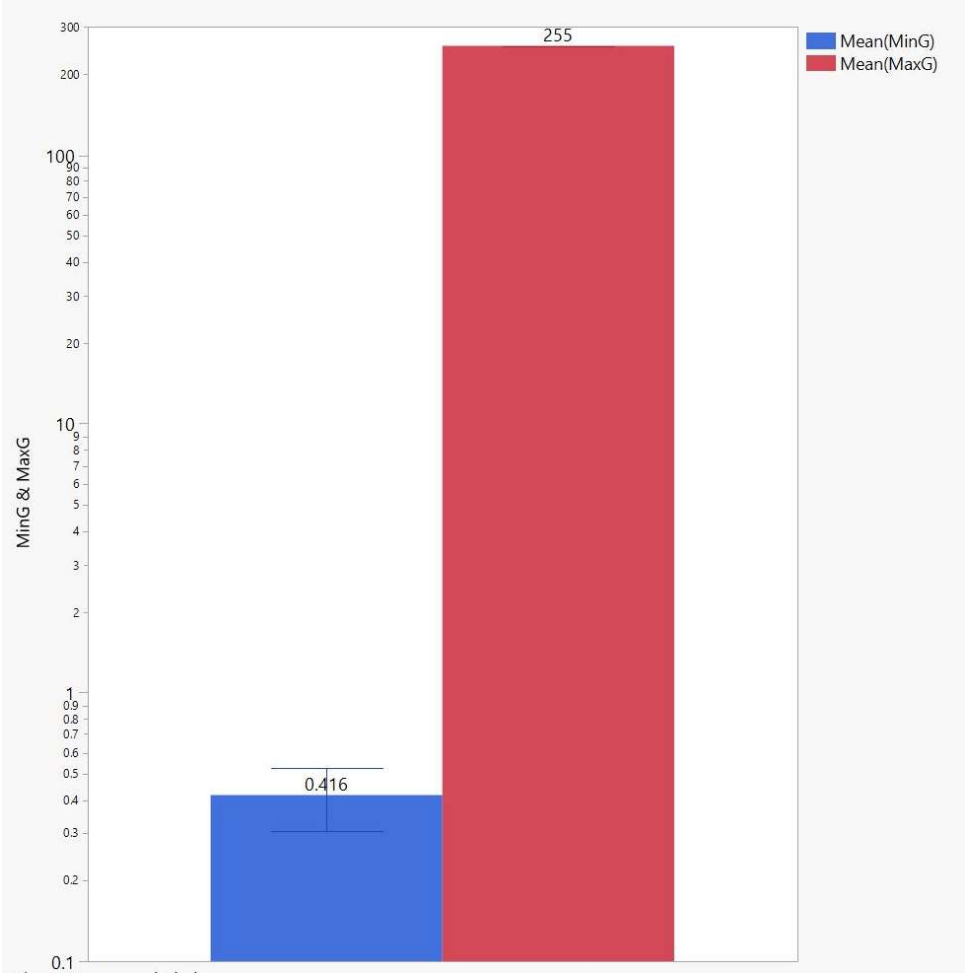

Figure 18: Experiment 1 Mean Minimum and Maximum Intensities.

Nucleus circularity is an additional parameter that seemed to be affected by treatment, Figure 19. Circularity output ranges from 0 (elongated shape) to 1 (perfect circle). Prior to UV irradiation, the nuclei circularity median was 0.64. Post UV irradiation, BSM treated nuclei had a circularity of 0.61 and No SM nuclei had a circularity of 0.57. This suggests UV irradiation negatively affects the circularity of nuclei and that the addition of BSM may help against that deformity.

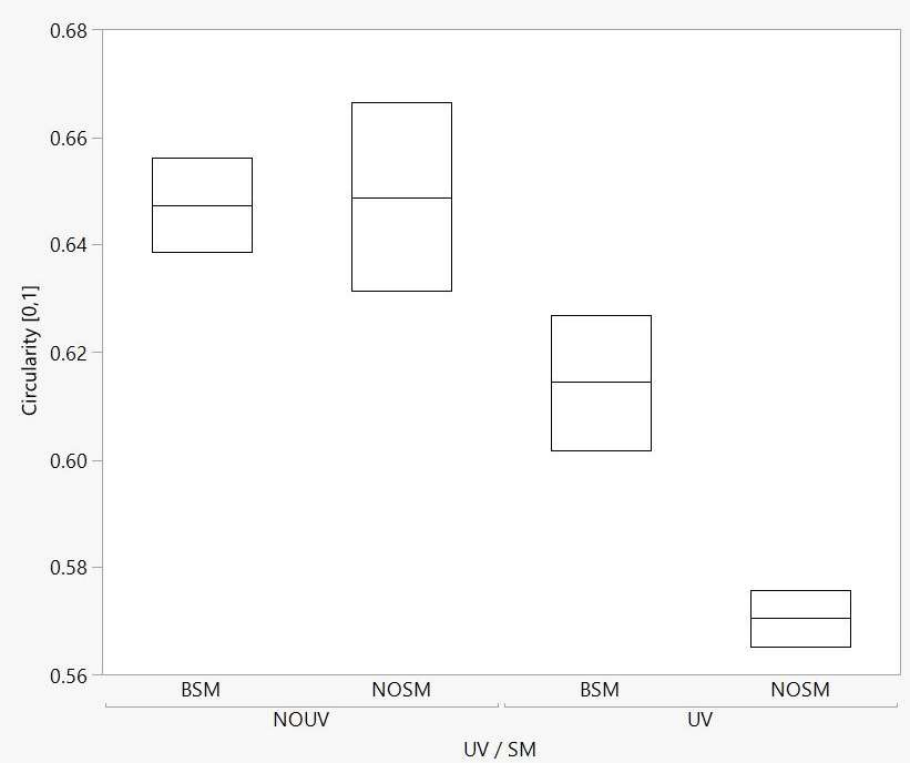

Figure 19: Experiment 1 Circularity.

4.1.3 Discussion

From the results of Experiment 1, previous lab's results were replicated and new parameters of interest were identified. Intensity values had to be normalized using cell count because variation in number of cells effected the overall intensity of each image. This variation in cell count was attributed to plate variation as well as BSM increasing the size of the cells. Qualitatively, cells looked appropriate and quantitatively, there was reduction of p21 damage when BSM was introduced.

Two, new parameters were found to be affected by treatment: min/max intensity values and nucleus circularity. Min and max ranges were estimated to serve as a filtering step for image abnormality. Additionally, nucleus circularity was negatively affected by UV irradiation. This correlation may also capture cell damage similar to p21 presence.

These parameters were reevaluated with a higher sample number to conclude differences with statistical power in Section 4.6.

4.2 FSM Treatment

4.2.1 Objectives/Methods

Sphingomyelin mechanism was not understood because BSM is unable to visualized within the cell. Fluorescent sphingomyelin (FSM) was proposed to be an analog to BSM with the additional ability to be visualized under confocal microscopy. The objective for Experiment 2 was to find equivalence between FSM and BSM by replicating previous FSM procedure with a new secondary and comparing their intensities. FSM and current p21 secondary shared a common emission spectrum. A new secondary was needed to separately analyze FSM and p21 intensity, illustration shown in Figure 8.

Goal 1: Replicate FSM procedure

FSM was introduced as an equivalent to BSM to better understand sphingomyelin's interactions within the cell. FSM's concentration was previously optimized, however, imaging was needed to confirm its equivalence.

Goal 2: Introduce new secondary AF 594

A new secondary was needed to visualize both the FSM and p21 antibody. Goat, anti-rabbit IgG AF 594 was a new secondary, and one treatment group was stained using Secondary AF 594 in order to provide comparison to Experiment 1. The procedure between the different secondaries were not changed. This experiment highlighted differences in p21 positive fluorescence between the secondaries.

The factors to evaluate were sphingomyelin, UV irradiation, and secondary antibody. Treatments were separated by plate and they were the following: A - No SM + No UV + Secondary AF 594, B - No SM + UV + Secondary AF 594, C - No SM + No UV + Secondary AF 488, D - No SM + UV + Secondary AF 488, E - FSM + No UV + Secondary AF 594, F - FSM + UV + Secondary AF 594, G - BSM + No UV + Secondary AF 594, H - BSM + UV + Secondary AF 594, shown in Figure 20. If BSM and FSM were equivalent, treatments E, F, G, and H were hypothesized to the same. Additionally, if secondaries were equivalent, treatment A/C and B/D would share similar trends.

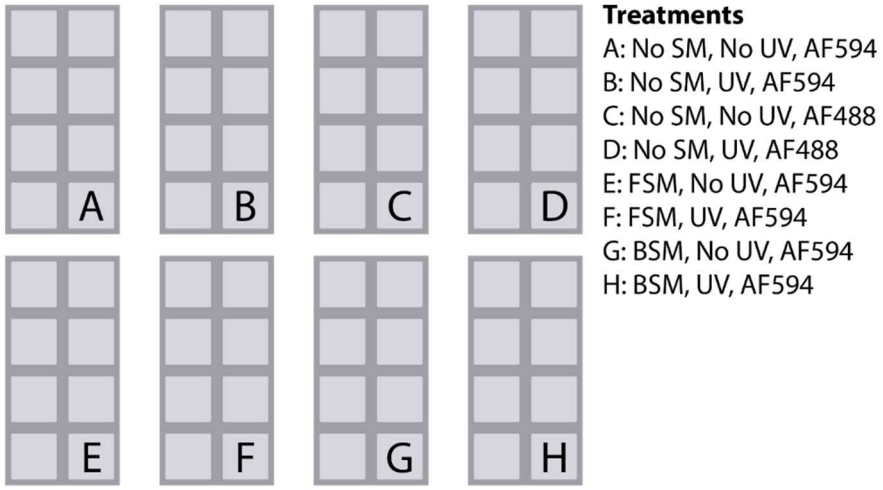

Figure 20: Design of Experiment 2. There was total of 8 plates and 8 treatments with each plate receiving a different treatment.

4.2.2 Results

There were differences between intensities for the new substrates. Laser power had to be reduced from 18% to 5% to prevent oversaturation of the FSM and initially, the new secondary did not appear to be present in the well using previous settings from Secondary AF 488. Secondary AF 594 was not seen until the high voltage (HV) was increased from 700 to 900. The optimal settings for this experiment can be summarized

in Table 3. After settings were determined, all three channels displayed distinct stains; Figure 21A shows nuclei in the DAPI channel, Figure 21B shows FSM in the AF 488 channel, and Figure 21C shows p21 presence in the AF 594 channel.

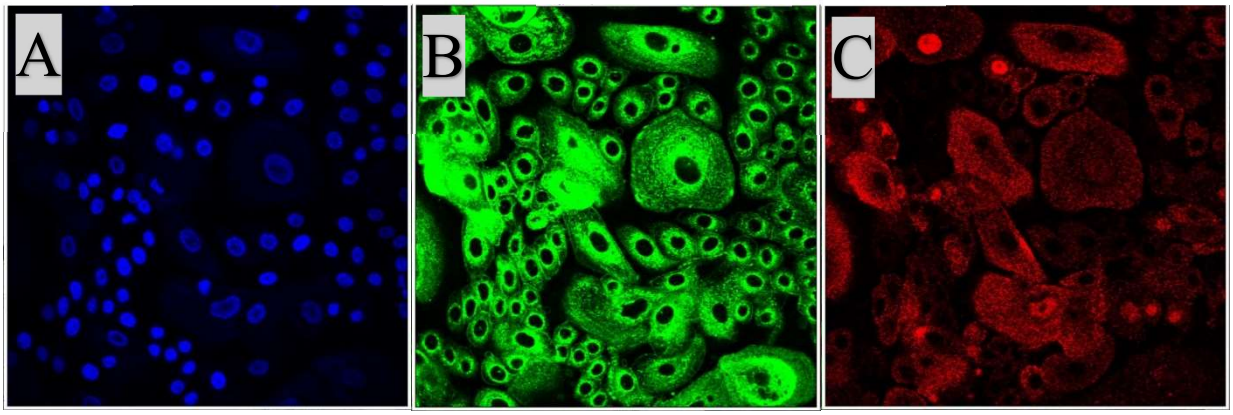

Figure 21: Experiment 2 Confocal Imaging. A. DAPI channel displays cell nuclei. B. AF 488 Channel displays FSM. C. AF 594 Channel displays p21.

After imaging was performed, images were processed, nested, and intensities were normalized by dividing by cell count. Figure 22 displays the different color p21 intensities as well as Experiment 1 results. In Figure 22A, there were no intensity differences between the Secondary AF 488 for Experiment 1 and Experiment 2 indicating experimental results were similar using the old secondary. This indicates that procedure was repeated sufficiently.

For Secondary AF 594, the expected results were no intensity differences between BSM and FSM. However in Figure 22B, Secondary AF 594 showed FSM treatment was not equivalent to BSM after UV irradiation. After UV irradiation, FSM treatment was equivalent in p21 postitive intensity as the No SM case with both having an intensity of 1 compared to BSM having an intensity of 0.6.

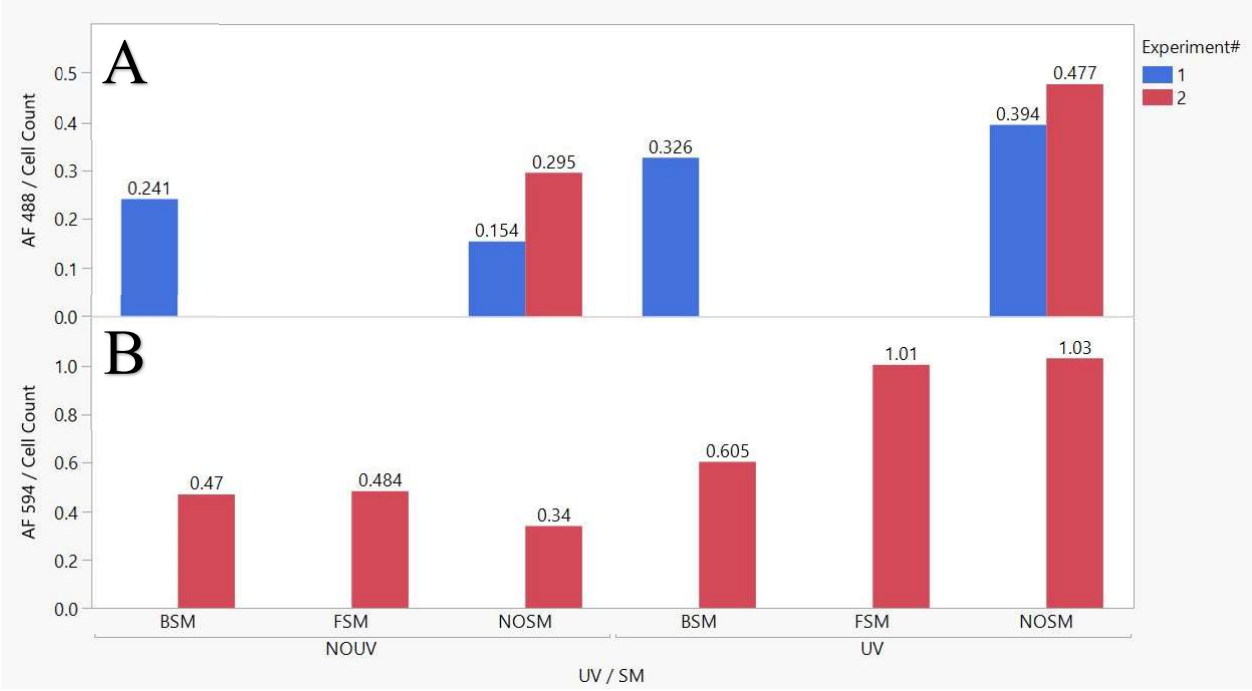

Figure 22: Experiment 2 p21 Intensity. A. Experiment 1 and Experiment 2 Secondary AF 488 intensities. B. Secondary AF 594 intensities.

4.2.3 Discussion

These results do not support the hypothesis that FSM and BSM carry the same protective effects. However, this may be due to the large differences in laser settings between channels. High voltage has an exponential relationship with the amount of energy introduced. There was a possiblity of involuntary excitation of the fluoro attached to FSM because the high voltage was so large in the AF 594 channel. This would cause the intensity of the p21 to increase to similar that of the No SM treatment.

Laser settings should be more closely related to the settings used for Secondary AF 488. This supports the need to optimize the secondary concentration. Additionally, once the concentrations are optimized, experimentation was needed to determine the appropriate incubation time so that FSM and BSM share the same protective properties.

The next series of experiments tried to address those issues. Experiment 3, Section 4.3, optimized Secondary AF 594 concentration and Experiment 4, Section 4.4, optimized sphingomyelin factor incubation time.

4.3 Optimizing New Secondary Concentration

4.3.1 Objectives/Methods

In the previous experiment above, Section 4.2, it was concluded that Secondary AF 594 concentration needed to be optimized. The main purpose for this experiment is to find the Secondary AF 594 concentration needed to visualize p21 presence and to evaluate if a reduction of Hoechst concentration prevents oversaturation. Ideally, the same laser settings as Secondary AF 488 should be used.

Goal 1: Optimize for new Secondary AF 594

Secondary AF 488 concentration does not translate sufficiently when Secondary AF 594 is used. A new concentration is needed to better capture Secondary AF 594 with similar laser settings to that of Secondary AF 488.

Goal 2: Evaluate reduction of Hoechst concentration

Current DAPI channel laser settings remain at a low power, but nuclei tend be oversaturated with minor adjustment. The Hoechst concentration should be reduced from 0.03% to 0.015% in order to decrease the likelihood of oversaturation. Confirmation is needed that these results will be sufficient to detect nuclei.

Protocol was replicated with all concentrations the same except for the Secondary AF 594 and Hoechst. No sphingomyelin treatment was added to produce the highest p21 positive concentration after UV irradiation. All plates received the reduced Hoechst

concentration of 0.015%, and the four different secondary concentrations evaluated were: 1:100, 1:200, 1:300, and 1:400, summarized in Figure 23. The expected result was to find a concentration with high intensity after UV irradiation and low variability within the plate.

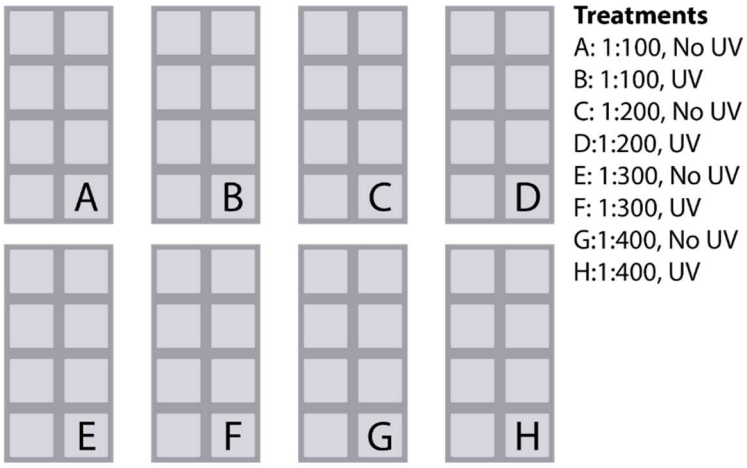

Figure 23: Design of Experiment 3. There were 8 plates and 8 treatments with each plate receiving a different treatment.

4.3.2 Results

Experiment 3 tried to find the concentration resulting in low variation between wells and better contrast of p21 positive intensity with less laser power. Laser settings for AF 594 channel were adjusted to share similar settings to Secondary AF 488 specified in Table 3. In Figure 24A, nuclei were clearly present in the DAPI channel. Qualitatively it was confirmed that reduction of Hoechst concentration did not affect visualization of nuclei and reduced the risk for oversaturation. In Figure 24B, AF 594 was able to detect red pockets of intensity which corresponded to p21 positive cells for all concentrations. Further analysis was needed to quantitatively find the highest concentration with the lowest variability. Three images were taken in the center of each well.

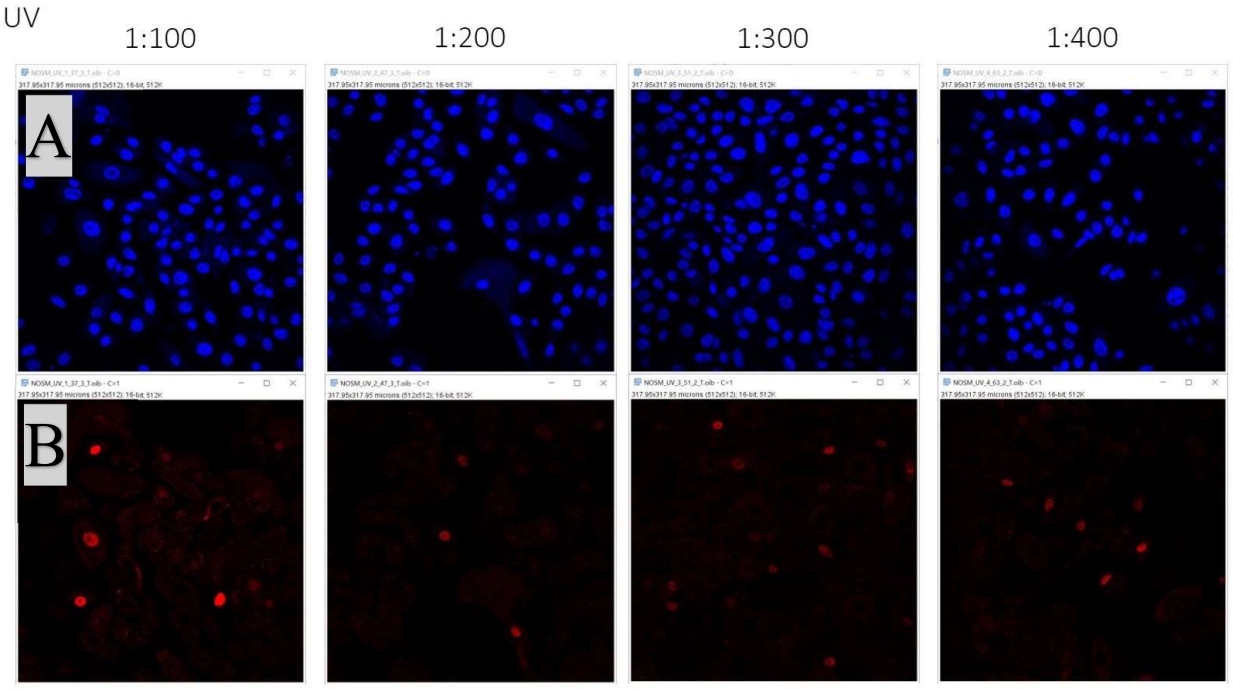

Figure 24: Experiment 3 Confocal Imaging. All images displayed derived from plates exposed to UV irradiation. Each column represents a different secondary concentration. A. DAPI channel display cell nuclei. B. AF 594 channel displaying p21 presence within cell.

Images were processed, averaged per plate, and normalized by p21 intensity by cell count, Figure 25. After UV irradiation, the three concentrations, 1:200, 1:300, 1:400, were not significantly different having intensity range of 0.046 to 0.062. The concentration 1:100 had the highest intensity per cell, indicating the highest p21 damage. However, it also had the largest variation meaning that there were other confounding factors that could be responsible for its high intensity.

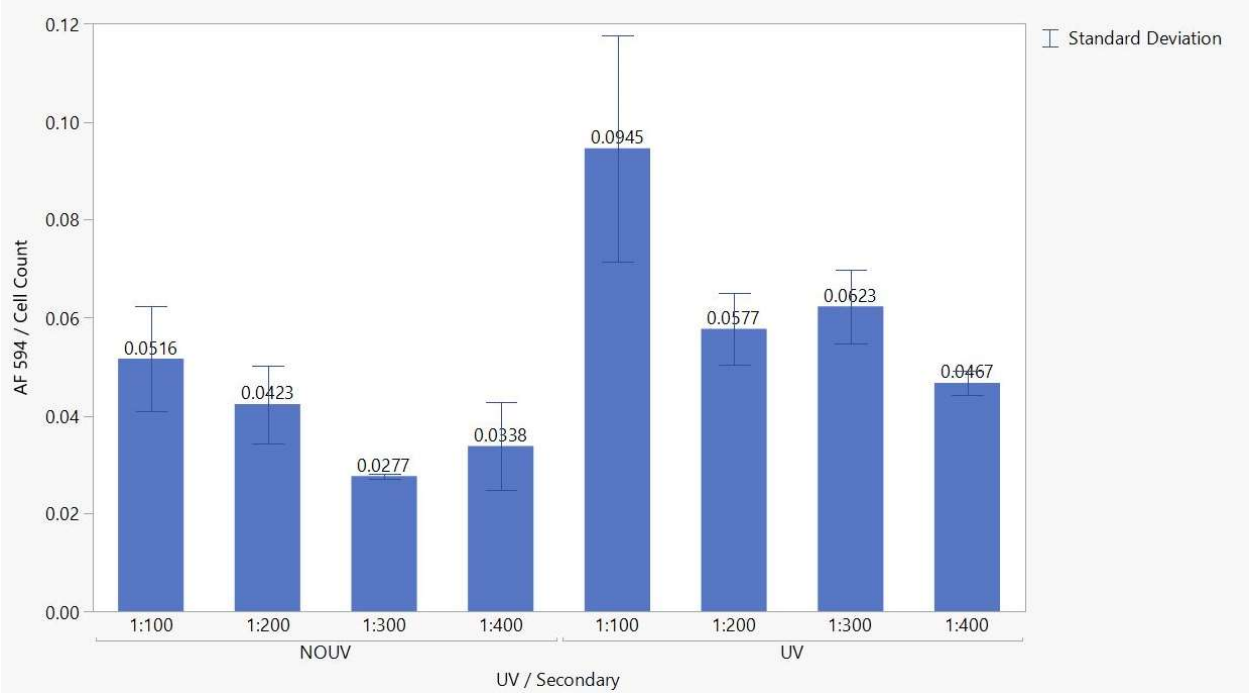

Figure 25: Experiment 3 Intensity. Average intensity was plotted per treatment along with their standard deviations.

4.3.3 Discussion

While having a too low concentration can prevent visualization of marker, a too high concentration could have adverse effects as well. A too high concentration can flood the area with markers that negate blocking solution and lead to non-specific binding. Additionally, high concentration lead to high costs. Finding the balance between intensity and variability is an appropriate method for determining optimal concentration. Therefore, concentration 1:100 was determined as too high of a concentration.

Ultimately, a concentration of 1:200 qualitatively showed the best results. It was also determined that secondary AF 488 still showed a better contrast. Therefore, Secondary AF 594 with a concentration of 1:200 should only be used to determine BSM-FSM equivalence for sphingomyelin location effort; Secondary AF 488 should be used for all other BSM-NoSM comparison.

4.4 Optimizing Incubation Time

4.4.1 Objectives/Methods

In a previous experiment above, Section 4.2, it was concluded FSM and BSM did not share the same photoprotective properties when using a 24 hour incubation period. There is an added aspect of external variability as incubation time increase. This experiment's focus to is determine a reduced incubation time that would show FSM and BSM equivalence.

Goal 1: Optimize FSM incubation with new Secondary AF 594 concentration

After finding the optimal concentration of Secondary AF 594, incubation time of FSM and BSM was reevaluated. The best incubation time would be where intensities of BSM and FSM are similar with low variation within plates. Additionally, results should replicate the trend of Experiment 1 in which UV treated plates have similar intensities to No UV case indicating introduction of BSM/FSM helps reduce cell damage.

The factors for this experiment included sphingomyelin (FSM or BSM), UV irradiation, and incubation time of sphingomyelin. A full factorial resulted in 16 different treatments, Figure 26. Each plate contained half wells with BSM and the other half with FSM. This ensured that plate to plate variation did not contribute to the variation observed in BSM and FSM. Previously, incubation was done at 24 hours and this incubation time should ideally be reduced to decrease variability among plates. Four incubation times were evaluated: 1 hour, 2 hours, 12 hours, and 24 hours. In order to limit the amount of additional variation, all steps except the FSM and BSM introduction should be performed approximately the same time. Therefore, plates first reached 70% confluency then incubation of BSM and FSM was done from longest to shortest (ie.24

hours, then 12 hours, etc.). At each treatment time, all plates were taken out of incubator to ensure that all plates had the same growing conditions.

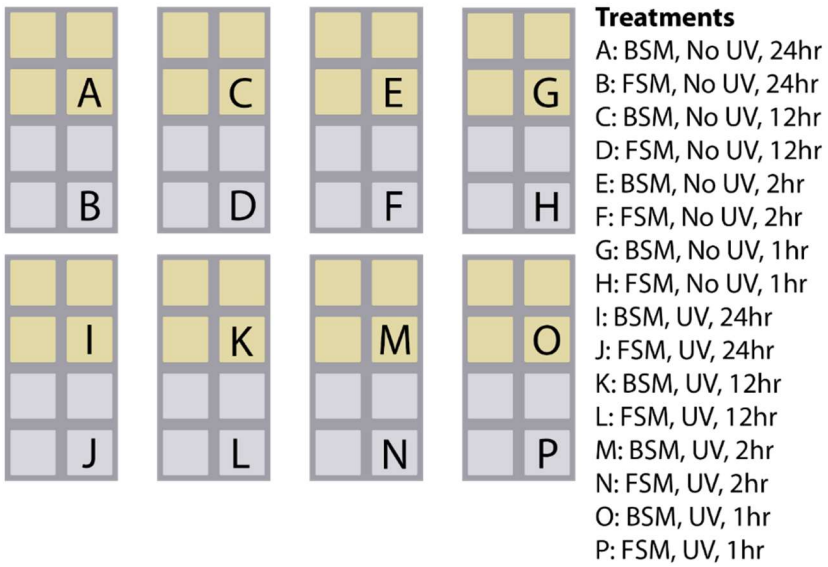

Figure 26: Design of Experiment 4. There were 8 plates and 16 treatments with each plate receiving two different treatments.

4.4.2 Results

Experiment 4 tried to find the most appropriate time BSM and FSM media should be exposed to keratinocytes to produce protective effects. It aimed to understand the time needed for proper intake of the sphingomyelin as well as if prolonged exposure could cause negative effects.

The process of UV irradiation and fixing remained the same, however, immunostaining was updated to optimize fluorescence parameters from Experiment 3 (i.e. Secondary AF 594, 1:200 and Hoechst, 0.015%), Section 4.3. Qualitatively, differences in intensities were comparable among the different treatments, Figure 27.

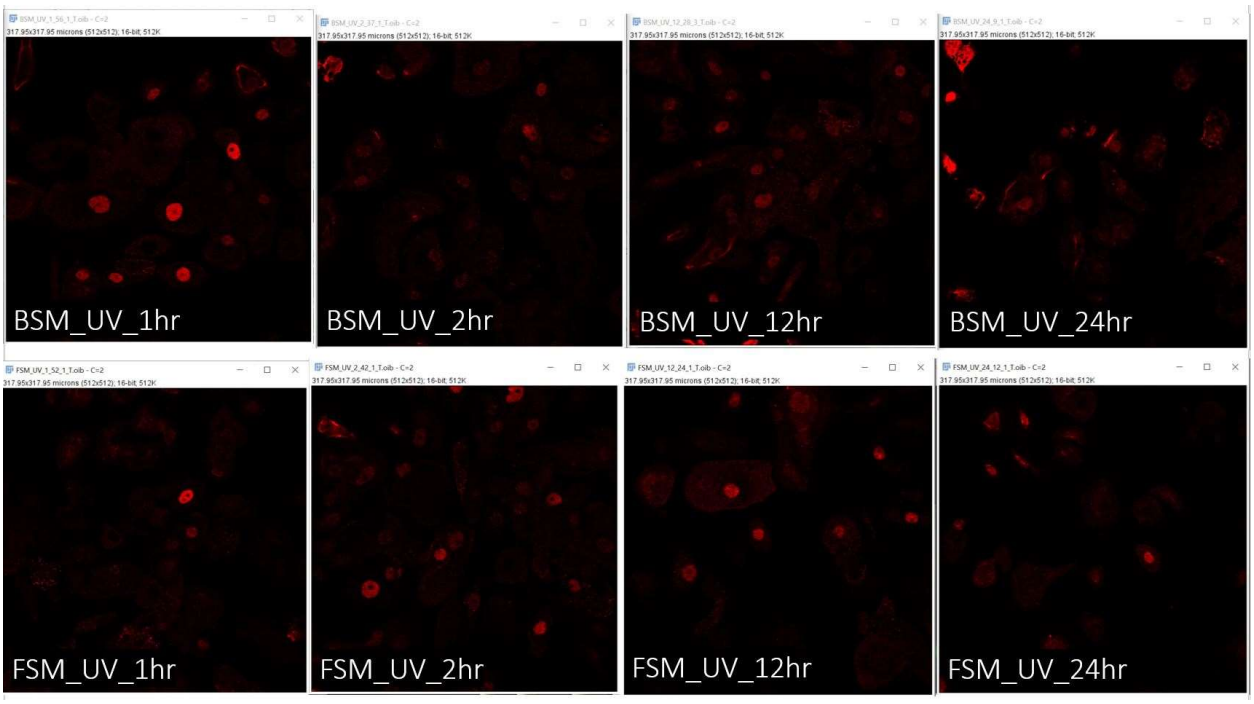

Figure 27: Confocal imaging of AF 594 channel.

Plates were then imaged, processed, and averaged. The intensity was divided by cell count to normalize results. Initial results showed that there were no significant differences between the No UV plates and differences among the incubation times after UV; Figure 28 shows No UV treatment to share an intensity range of around 0.10 to 0.13 (i.e. an interval of no greater than 0.3).

Because there were no differences in the No UV case, determination of optimal incubation time was then pivoted to only UV treatments. FSM and BSM intensities were similar when isolated by incubation time expect for the 1-hour timepoint. At 1 hour, BSM had an intensity of 0.264 compared to FSM with 0.127. This indicated that BSM is slower to uptake than FSM and it may be due to small differences in molecular structure. At 2 hours, intensities between FSM and BSM were not significantly different and standard deviations were low. At 12 hours, there is was an increase in intensity for both sphingomyelin treatments. It is unclear what caused this rise, but it may be due to

decrease in activation of sphingolipid ceramide pathway at that specific time point. Lastly at 24 hours, shared similar results to 2 hours, however, that increased experimental time can add externally variability to the results.

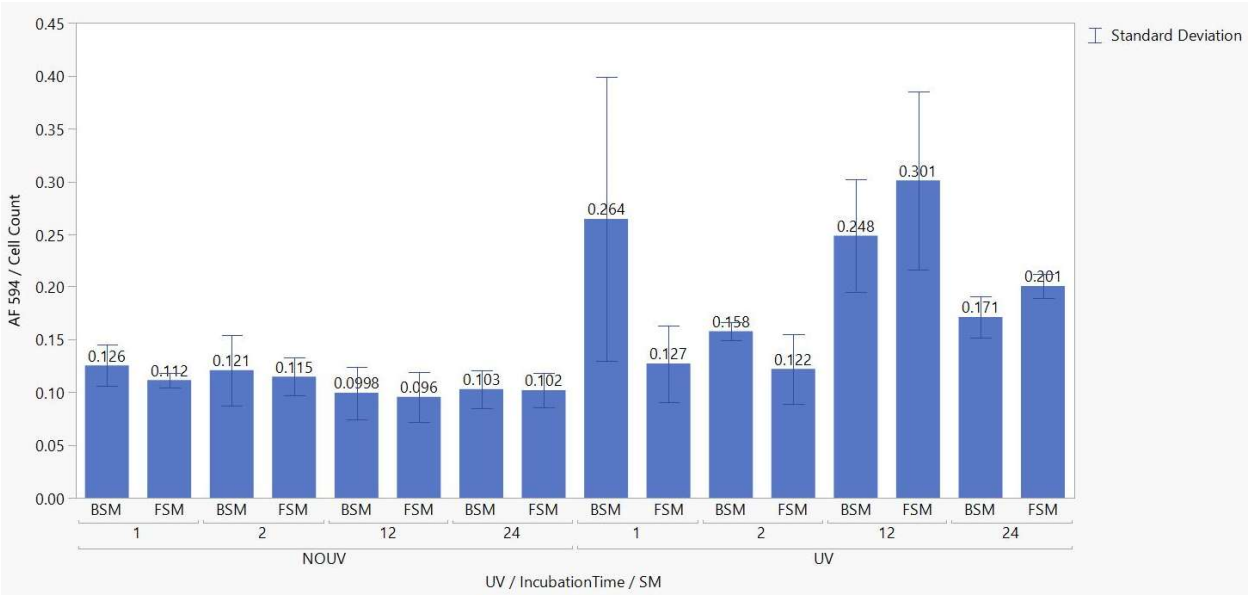

Figure 28: Experiment 4 Intensity. Mean intensities were plotted as well as their standard deviation.

4.4.3 Discussion

Experiment 4 tried to find the optimal incubation time required for BSM and FSM equivalence with the most photoprotective effects. If sphingomyelin did protect the cells, their intensities should be equivalent to the No UV case. Results showed that incubation for 2 and 24 hours had the lowest increase in intensity as well as BSM and FSM shared similar results. Final determination of incubation was based on reducing experimental variation. The longer sphingomyelin is incubated the increase of variation due to environmental factors, such as incubation conditions and cell growth. Because both time points had equivalent intensities, the 2-hour incubation should be used to limit variation and overall decrease experimental time and resources.

4.5 FSM Localization

4.5.1 Objectives/Methods

In the previous experiment above, Section 4.4, a 2-hour time point was concluded to be the optimal time for FSM and BSM incubation. The main purpose of this experiment was to confirm FSM and BSM equivalence and to investigate the location of FSM. Additionally, Secondary AF 488 was used for some BSM and No SM treatments to compare results to previous experiments.

Goal 1: Compare FSM and BSM

Further experimentation comparing BSM and FSM is needed using the improved protocol from Experiment 3 and Experiment 4, Section 4.3 and 4.4 respectively. These changes include a 2-hour sphingomyelin treatment time, increased concentration of Secondary AF 594, and reduced concentration of Hoechst to 0.015% to optimize for imaging parameters.

Goal 2: Observe the distribution of FSM within keratinocytes

Sphingomyelin mechanism is still unknown. Figuring out its location before and after UV irradiation can help understand its mechanism of protection against cell damage. FSM allows visualization under confocal imaging. If FSM and BSM are comparable, localization efforts of FSM can allow hypothesis of mechanism of sphingomyelin.

Because Secondary AF 488 showed a better contrast compared to Secondary AF 594, half of the plates were stained with Secondary AF 594 for BSM and FSM comparison and the other half were stained Secondary AF 488 to confirm appropriate staining technique compared to previous experiments. Figure 29 shows the 8 different

treatment evaluated: A – No SM + No UV + Secondary AF 488, B – No SM + UV + Secondary AF 488, C – FSM + No UV + Secondary AF 594, D – FSM + UV + Secondary AF 594, E – BSM + No UV + Secondary AF 488, F – BSM + UV + Secondary AF 488, G – BSM + No UV + Secondary AF 594, and H – BSM + UV + Secondary AF 594. If hypotheses were assumed correct, treatments C/G and D/H should be equivalent, treatments E/G and F/H should share the same trend, and treatments A/B/E/F should be equivalent to previous experimentation.

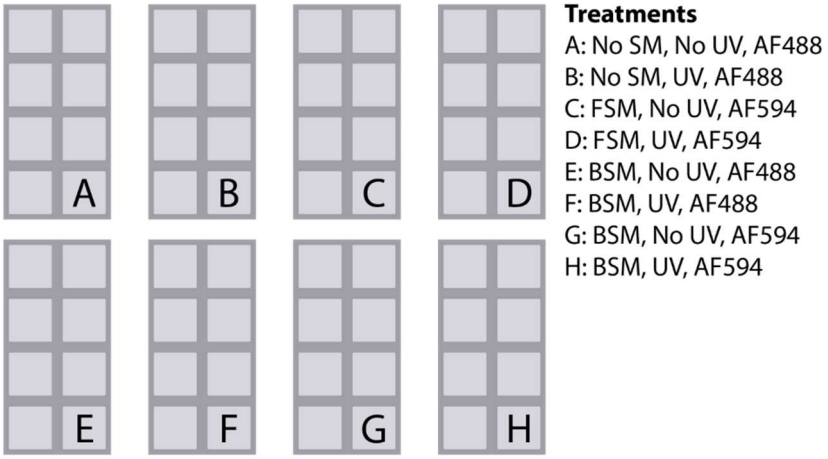

Figure 29: Design of Experiment 5. There were 8 plates and 8 treatments with 4 plates receiving Secondary AF 488 and the other receiving Secondary AF 594.

4.5.2 Results

Plates were imaged, processed, and averaged before data analysis. Because intensity range between secondaries were different, plates were separated by secondary type. Intensities were normalized by dividing cell count.

There was insufficient evidence to conclude a difference between BSM and FSM using Secondary AF 594, Figure 30. Their means are slightly different between treatments, but their standard deviations overlap each other giving the possibility that their true means may be the same. Furthermore, there was no significant difference

between UV and No UV treatment. This indicates FSM and BSM are comparable as well as they may have protected plates from p21 damage during UV irradiation. There was no control case (i.e. No SM) that was stained with Secondary AF 594, however, the No SM + UV treatment was observed to exceed the intensities in the BSM and FSM case.

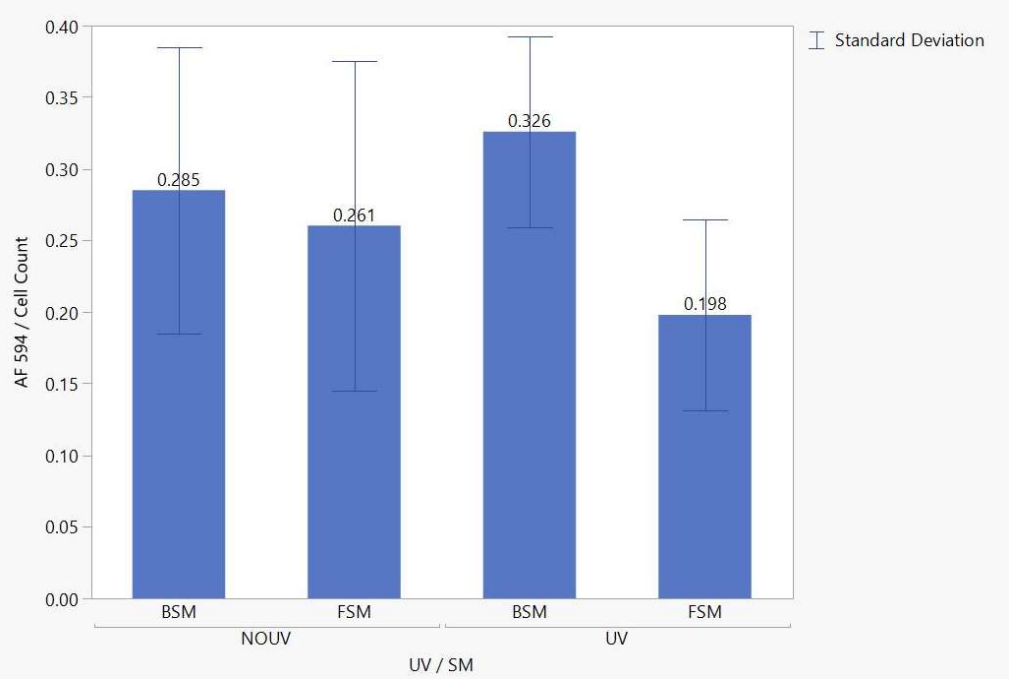

Figure 30: Experiment 5 AF 594 Intensity. Average intensity values were plotted as well as their standard deviations.

When we observed the plates stained with Secondary AF 488, we expected to see a large increase in intensity for No SM + UV case. However when examining intensities using Secondary AF 488, there was not a significant difference between all treatments, Figure 31. Similar to Secondary AF 594, their standard deviations overlapped each other. This means it cannot be concluded whether their true means were different or the same. Although direct true mean differences cannot be compared, their sample means did show an increase of 0.065 for the No SM case and a decrease of 0.005 using BSM after UV irradiation. This supports the hypothesis that BSM provides protective benefits against

UV irradiation. In order to gain statistical power for this hypothesis, more samples were needed to better estimate the true mean treatment population and variation of the data must be reduced.

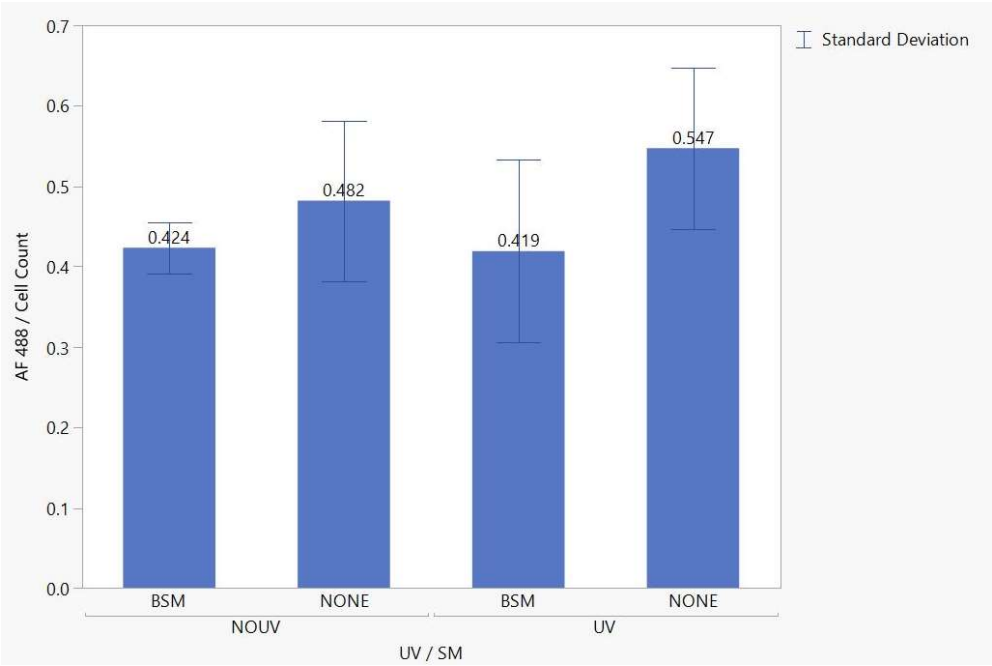

Figure 31: Experiment 5 AF 488 Intensity. Average intensity values were plotted as well as their standard deviations.

Qualitative analysis using the FSM channel attempted to visualize sphingomyelin within the cell. The confocal microscope enabled with a 100x objective was used to capture images of cells with higher magnification allowing for greater specificity. Images were made binary, an ellipse was formed around one cell, a Gaussian Blur filter was applied (Section 3.7.4), and a surface plot was created, shown in Figure 32. A surface plot takes the intensity of each pixel and plots it in a 3-dimensional matrix. The DAPI channel was compared to determine the location of the cell's nucleus, and FSM did not appear to be located within the nucleus. The surface plot showed FSM intensity to be high around the nucleus' perimeter and gradually diminish as analysis traveled radially

outward. There appeared to be a low concentration of fluorescence at the cell's outer lipid membrane.

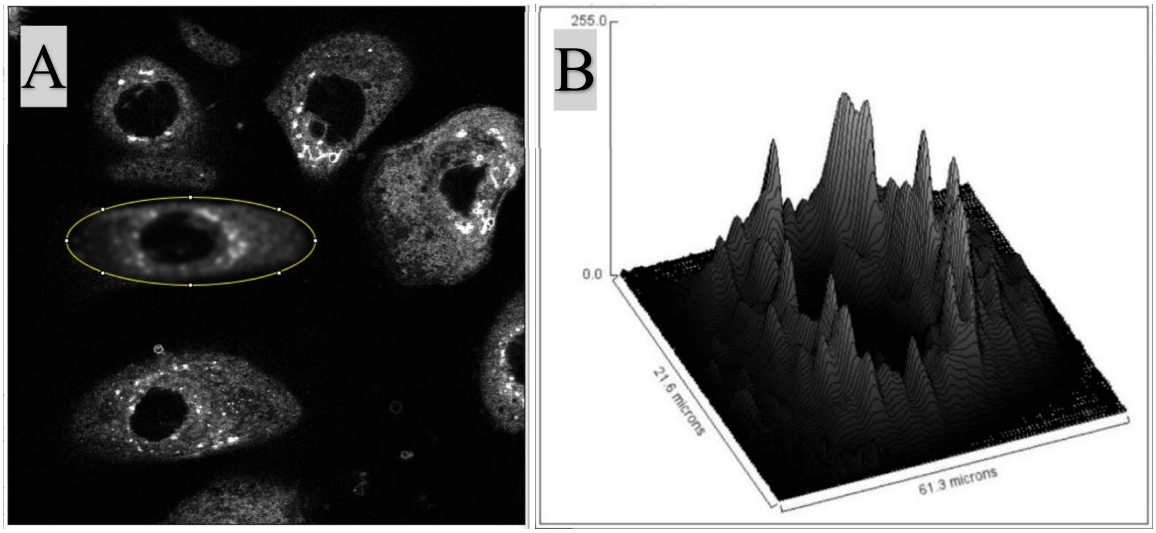

Figure 32: Surface Plot of FSM Location within Cell. A. Cell image at 100x magnification. An ellipse, shown as yellow, surrounds the cell of interest and Gaussian Blur filtered the inside of the ellipse. B. Surface plot of the ellipse with peaks being areas of high fluorescence.

Because a cell is somewhat radially symmetrical, a slice starting from the center of the nucleus extending across its cytoplasm to the outer lipid membrane allowed a 2-dimensional trace of intensity. A new rectangular area of interest was created, Gaussian blur was applied, and a profile plot was created. A profile plot analyzes that pixel's intensity versus its distance relative to how far it is from the leftmost rectangular line. Multiple cells were analyzed; Figure 33A is the 2nd image taken from a well with treatment FSM + UV and Figure 33B is the 3rd image taken from the same well. Cell variation such as size, circularity, count, etc limited the grey values range from matching exactly from cell to cell; this did not allow for direct grey value comparison. The same observations were seen in profile as with the surface plot with highest FSM concentration closest to the nucleus and low concentration at the cell's lipid membrane.

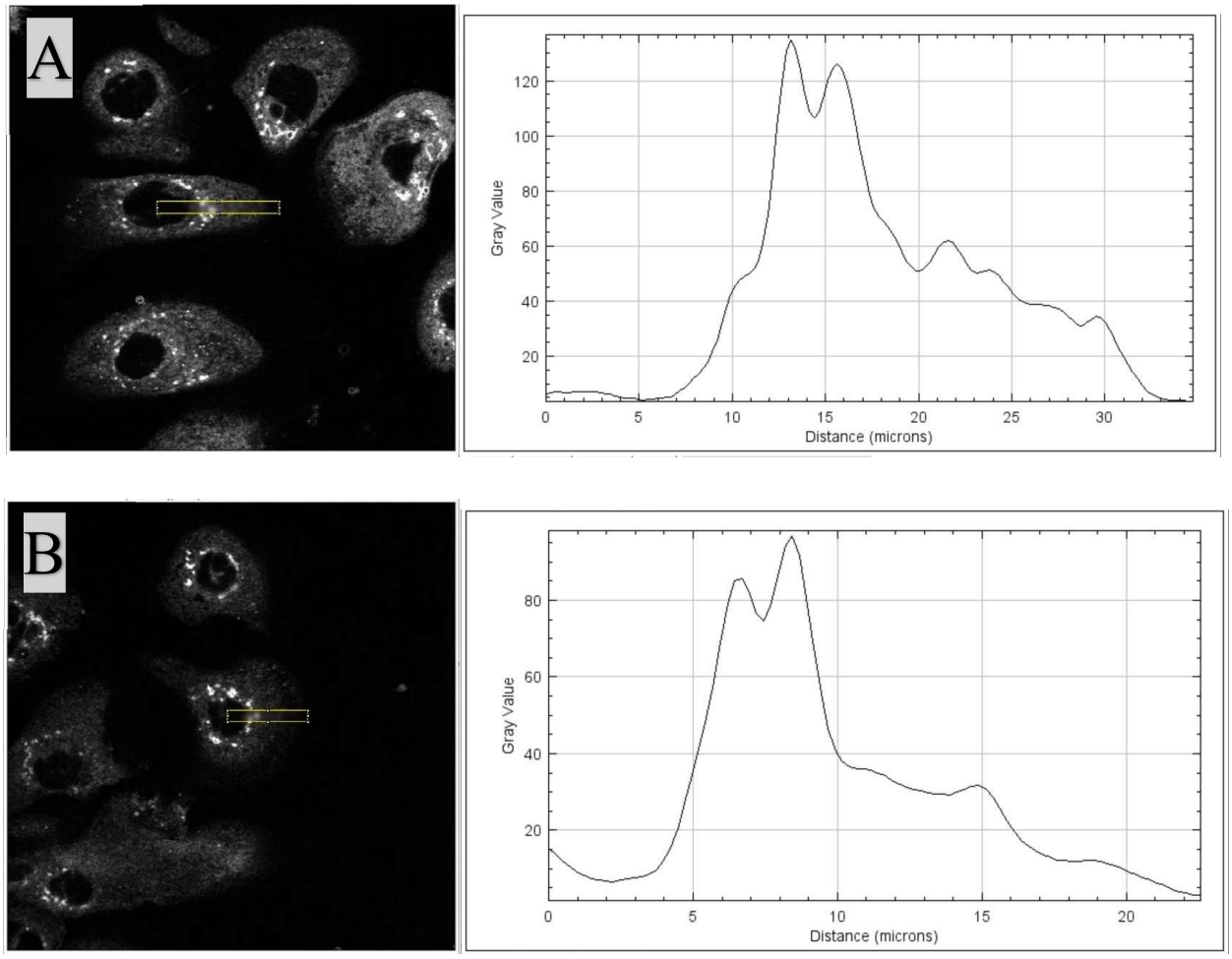

Figure 33: Profile Plot of FSM Location within Cell at 100x. A and B are different cells of interest on different images. Yellow boxes for the profile plots are drawn starting from their nucleus to their outer lipid membrane. Their corresponding profile plots are on their right.

4.5.3 Discussion

This experiment tried to confirm FSM and BSM equivalence and confirm results seen in previous experimentation. Although large standard deviations caused insufficient statistical significance, observationally the p21 intensities were equivalent among BSM and FSM cases stained with Secondary AF 594. Additionally, BSM and No SM cases stained with Secondary AF 488 showed similarities with previous experimentation with the No SM + UV treatment having a higher intensity then the BSM + UV treatment.

When observing at 100x magnification, there was high cell variation within images as well as between images. However, there was a trend in FSM intensity seen in the surface plot. FSM had the greatest concentration in the area surrounding the nucleus. Because sphingomyelin is hydrophobic, FSM is most likely localized in vacuoles this is seen as globular pockets of fluorescence along the nucleus.

The following is a proposed mechanism of sphingomyelin. Sphingomyelin enters cell membranes and disrupt well-formed lipid rafts. This disruption causes a significant decrease in UV-induced reactive oxygen species (ROS) synthesis. Additionally, sphingomyelin breaks down into ceramide and caused ceramide-dependent activation of PKCζ [70]. This provides the benefit of reduction in p21 upregulation, reduction of apoptotic markers such as DNA fragmentation, and causes an increase in epidermal proliferation upon UV irradiation [71].

4.6 Experiment Replication with Updated Protocol

4.6.1 Objectives/Methods

The purpose this experiment was to reach statistical significance with the trends observed in Experiment 1 or at the very least record some of the unexplained variation. The protocol found in Appendix A was modified to enhance these trends while reducing intra-subject standard deviation, Experiments 2 - 5.

Goal 1: Replicate previous experimentation results using new substrates, materials, and slightly modified procedure.

Significance between BSM and No SM was not concluded in Section 4.5 because of the limited sample size. In Experiment 5, the protocol was updated to optimize for

equivalence of BSM and FSM effects. Therefore, replication of the Section 4.1, with the updated protocol, was needed to understand the variation between results. If results were equivalent to Experiment 1, we expected to see a large intensity increase in No SM + UV treatment and low, equivalent intensities for all other treatments.

Goal 2: Understand variation between experiments

In order to confirm results similar to Experiment 1, low variation must be observed within plates and cell counts should be consistent with previous experiments. Additionally, we want to understand the variation between experiments. In this experiment, some immunostaining substrates came from a different batch. This can cause additional variation between experiments and ultimately affect results.

The main differences in protocol were a 2 hour sphingomyelin incubation time and reduction of Hoechst concentration to 0.015%. Because Secondary AF 448 yields a higher contrast between non and p21 positive cells, only Secondary AF 488 was used. Eight plates with keratinocytes were grown until at least 70% confluency. Then, Experiment 1 treatment groups were repeated (A – No SM + No UV, B – BSM + No UV, C – No SM + UV, and D – BSM + UV) using the updated protocol, seen in Figure 34.

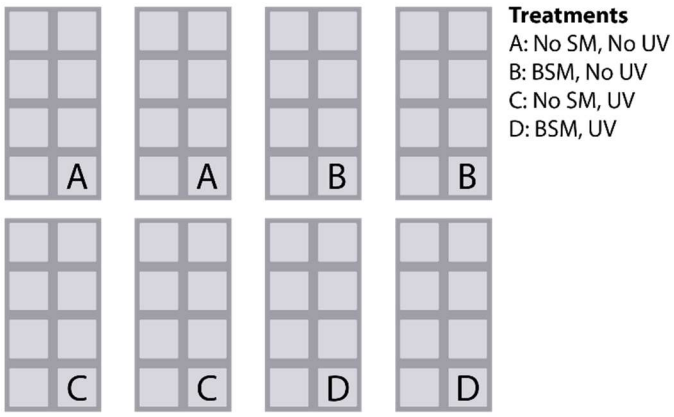

Figure 34: Design of Experiment 6. There were a total of 8 plates and 4 treatments with 2 plates receiving each treatment.

4.6.2 Results

This experiment attempts to understand the intra-subject variability of experiments. Differences were first observed during confocal imaging with one treatment case significantly differing in cell count compared to other treatment cases. Qualitatively, it was noted the BSM + UV plates had uncharacteristically less cells in its wells, Figure 35C. Furthermore, BSM + UV images may have had some nonspecific binding seen in Figure 35C where there was p21 fluorescence but no nuclei present in the DAPI channel corresponding to those areas.

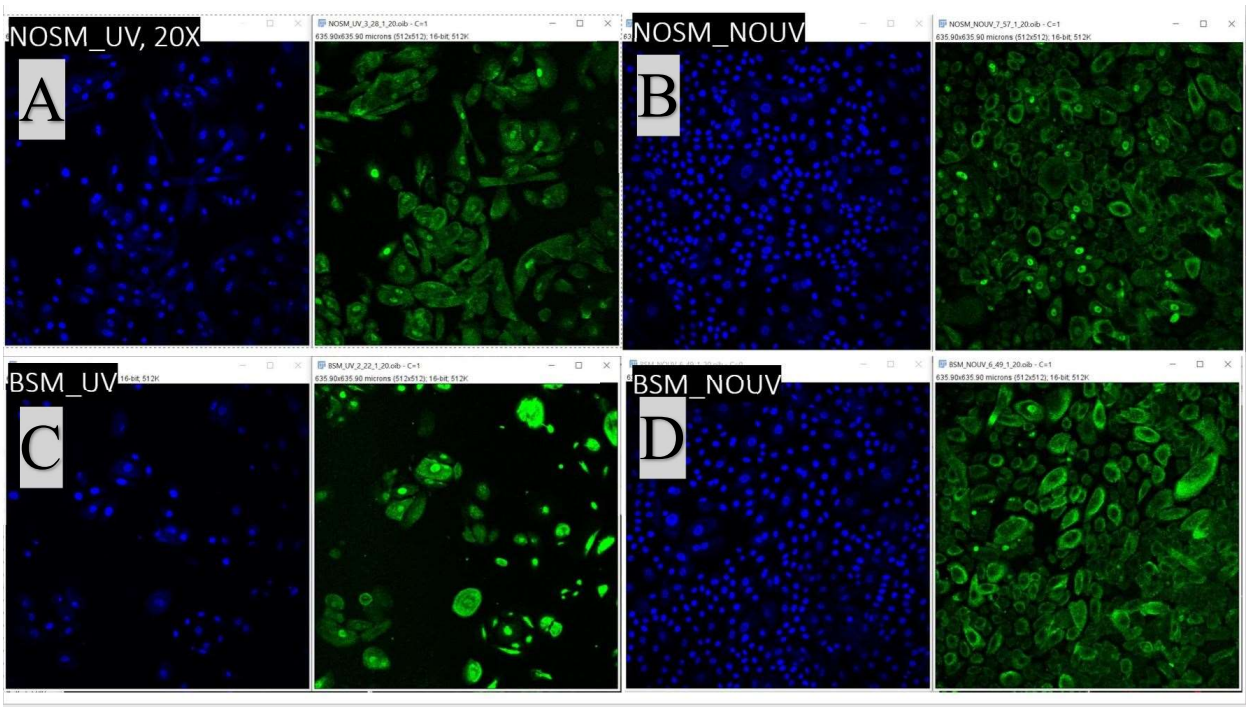

Figure 35: Experiment 6 Confocal Imaging. Using a 20x objective, a larger portion of well was observed. The DAPI channel in blue displays cell's nuclei and the AF 488 in green displays p21 within cell. A. Image of well treated with No SM and UV irradiation. B. Image of well treated with No SM and No UV. C. Image of well treated with BSM and UV irradiation. There appears to be less nuclei compared with the other images. D. Image of well treated with BSM and No UV.

Images were then processed and averaged for data analysis. Figure 36 quantitatively shows that treatment BSM + UV had the lowest cell count with an average of 22 cells per image. While it is true, UV irradiation kills some cells, it not typical that BSM, pre versus post UV had a percent change of around 70%. This and the fact that the variability of cell counts was high among the plates, raised concerns of significance with results of p21 intensity.

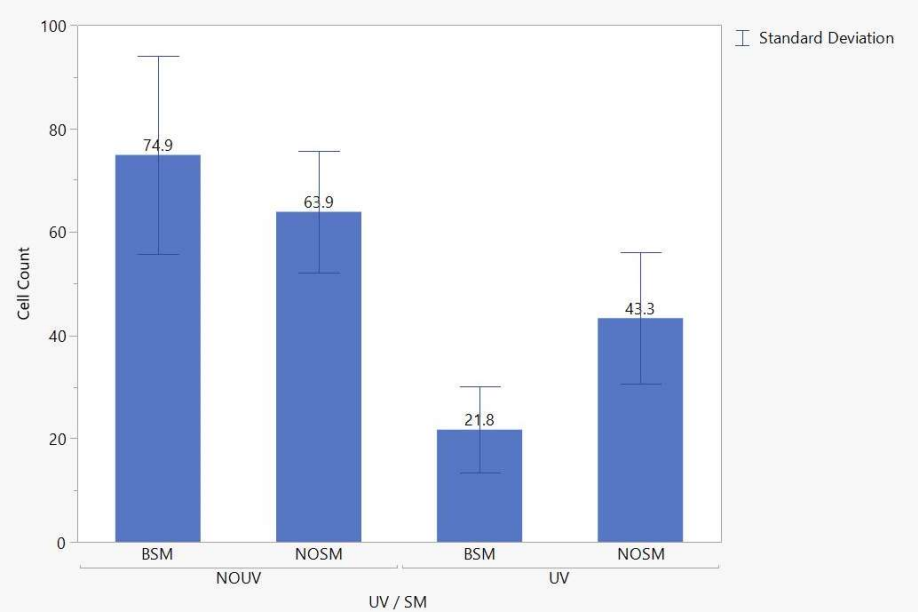

Figure 36: Experiment 6 Cell Count. Average cell count was plotted as well as their standard deviations.

P21 intensities were again normalized by dividing by cell count. Results showed that BSM increases p21 concentration compared to No SM + UV. This result is contradictory with Experiment 1, Figure 37.

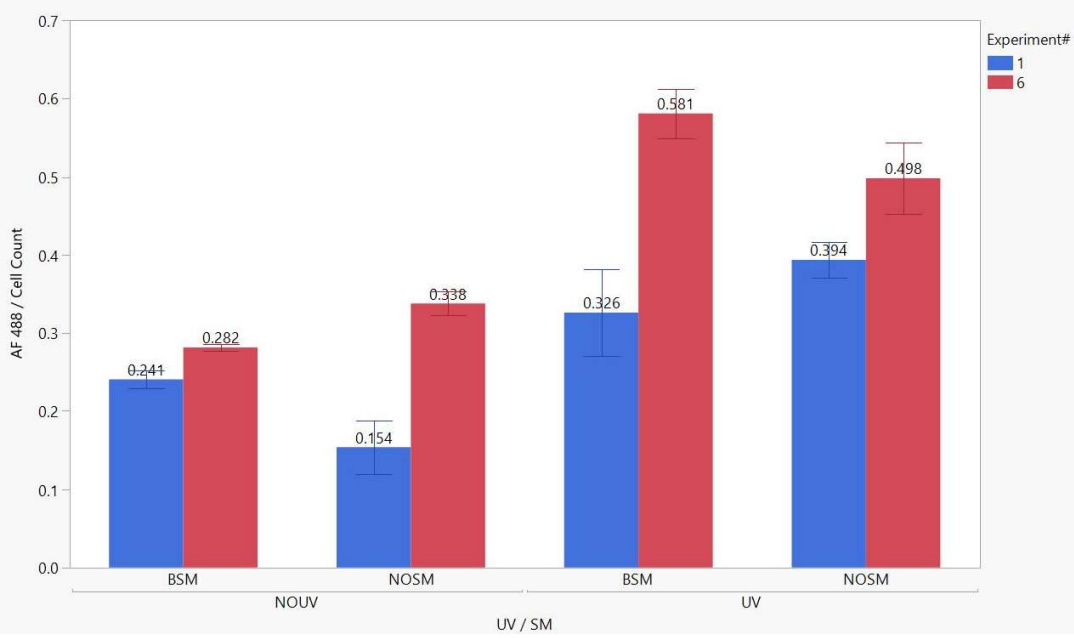

Figure 37: Experiment 6 AF 488 with for Experiment 1 for Comparison.

4.6.3 Discussion

The purpose of this experiment was to replicate Experiment 1 using an updated protocol. Due to concern of abnormal cell count and p21 fluorescence in the BSM + UV treatments, results were likely inaccurate. In the BSM + UV plates, cell count dropped about 70% and qualitatively images had some non-specific binding, shown in Figure 35C. The main source of error may be due to old cells with abnormal morphology. The keratinocytes that were seeded in these plates came from passage number 5 with prolonged time in the freezer. This can cause abnormal cell growth and may have contributed to their sensitivity when exposed with UV. This further highlighted the high intra-subject variation experienced between experiments.

4.7 Compiled Data Analysis

4.7.1 Objectives/Methods

One last meta-analysis was performed to understand variation between experiments and to evaluate experimental parameters found in Experiment 1. Experiment 1- 6 results were combined to gain a larger sample size and no new experiments were performed due to limited access to the lab because of COVID-19.

Goal 1: Understand inter and intra subject variation

Previous experimentation found that there was a difference between treatments, but their unexplained variation was large enough to negate significance. Further combination of experiments could yield a quantitative value for intra subject variation.

Goal 2: Evaluate treatment effects on experimental parameters and its significance

New experimental parameters were found in Experiment 1 to further analyze the difference between treatments. Because a large experimental study was not performed, combining experiments can understand correlations and significance of new parameters.

Goal 3: Estimate number of trials needed for statistical significance

By understanding the variation between experiments, the number of experiments needed to conclude significance was estimated. Currently, any statistical analysis performed on an individual experiment is not sufficient because it lacks degrees of freedom (i.e. statistical power).

4.7.2 Results

Variability within plates was something that greatly affected the precision of the data. This is unideal because high variability requires more samples to estimate the true population value. Mean intensities normalized by cell count and their standard deviations were plotted for all plates separated by experiment, UV treatment, and SM treatment, Figure 38.

The red rectangle in Figure 38 showed that plates stained with Secondary AF 594 in Experiment 2, Section 4.2, displayed larger standard deviations compared to the other experiments. This may be due to the lack of contrast from a subprime secondary concentration; variation was reduced as the secondary concentration was optimized in Experiments 2 and 3. Because variability from secondary was eliminated in later experiments, results from Experiment 2 was disregarded from compiled data analysis, recorded in Table 6. Variance was later used to estimate sample size, Section 4.7.2.6.

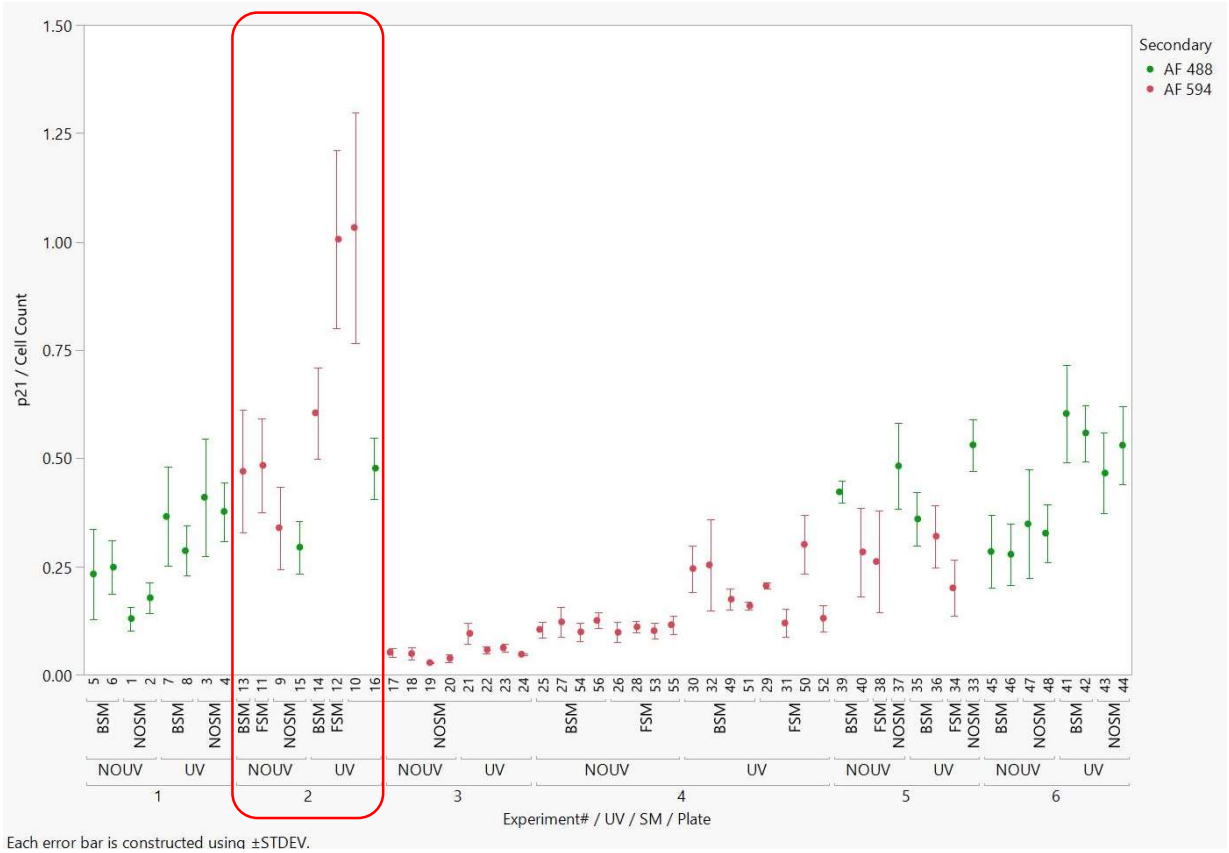

Figure 38: Experiment 7 Intensity Standard Deviations. Secondary AF 488 and Secondary AF 594 were differentiated. Red rectangle highlights Experiment 2 as having plates with larger standard deviations compared to other experiments.

Experiments 1- 6 were used for data analysis for a sample size of 56. However, 9 plates were excluded from analysis due to high or unexplained variability, summarized in Table 6, for total of n=20 with Secondary AF 488 and n=27 with Secondary AF 594. Analysis using the DAPI channel were combined between secondaries (n=47), but intensity analysis using secondaries were separated due to differences in contrast between fluorescence.

Table 6: Excluded Plates prior to Compiled Data Analysis (n=9).

Experiment	Treatment Plates Excluded	Reasoning
2 Section 4.2	No SM, No UV, AF 594 No SM, UV, AF 594 FSM, No UV, AF 594 FSM, UV, AF 594 BSM, No UV, AF 594 BSM, UV, AF 594	Unknown reason for high variability within plates, Figure 38. Secondary AF 594 needed to be optimized in order to image with appropriate laser settings and enough contrast.
3 Section 4.3	1:100, UV	Intensity was significantly different than the other concentrations. It also had a large standard deviation.
6 Section 4.6	BSM, UV (2x)	Abnormally low cell count due to harsh BSM application or some other unexplained variation.

Along with the cell count and p21 intensity, additional experimental parameters were evaluated from Experiment 1, Section 4.1. An explanation of the new parameters is found in Table 4. Table 7 summarizes the parameters evaluated as well as the main results concluded from analysis.

Table 7: Experiment 7 Summary of Results.

Parameter	Thesis Section	Results
Cell count	Section Cell Count 4.7.2.1	UV irradiation significantly lowers the cell count regardless of treatment. It is estimated the UV irradiation reduces cell count by 24%.
P21 intensity	Section 4.7.2.2	After normalizing by dividing by cell count, there is insufficient evidence to support the hypothesis that BSM has protective effects after UV irradiation.
Min and Max Grey Values	Section 4.7.2.3	Min and max values help determine if image contrast is abnormal, however, the range for filtering was adjusted and relaxed to reflect experimental data.
Circularity	Section 4.7.2.4	UV irradiation significantly lowers circularity of nucleus regardless of treatment.
Correlations	Section 4.7.2.5	Circularity correlated with perimeter and average size.

		Count correlates with Total Area.
Sample Size Estimation	Section 4.7.2.6	Because of large inter and intra variation, additional trials are needed to conclude significance with appropriate confidence.

4.7.2.1 Cell Count

Cell count was determined by counting the number of stained nuclei from the DAPI channel, Section 3.7.1. The cell count for each image was taken and the average cells per image was taken for each plate. With a sample size of n=47, there is sufficient evidence ($t < 0.0001$) to conclude a decrease in cell count after UV irradiation, Figure 39. Using the parameter estimates, it is estimated each well contains 78 cells per image and that UV irradiation removes 19 cells from each image. That reduction of 24% supports the need to normalize intensities by cell count and UV irradiation. Furthermore, 24% could serve as a metric to evaluate if UV irradiation was effectively administered. If cell count from pre to post UV irradiation differs substantially, it could be due to inadequate or too long UV exposure time.

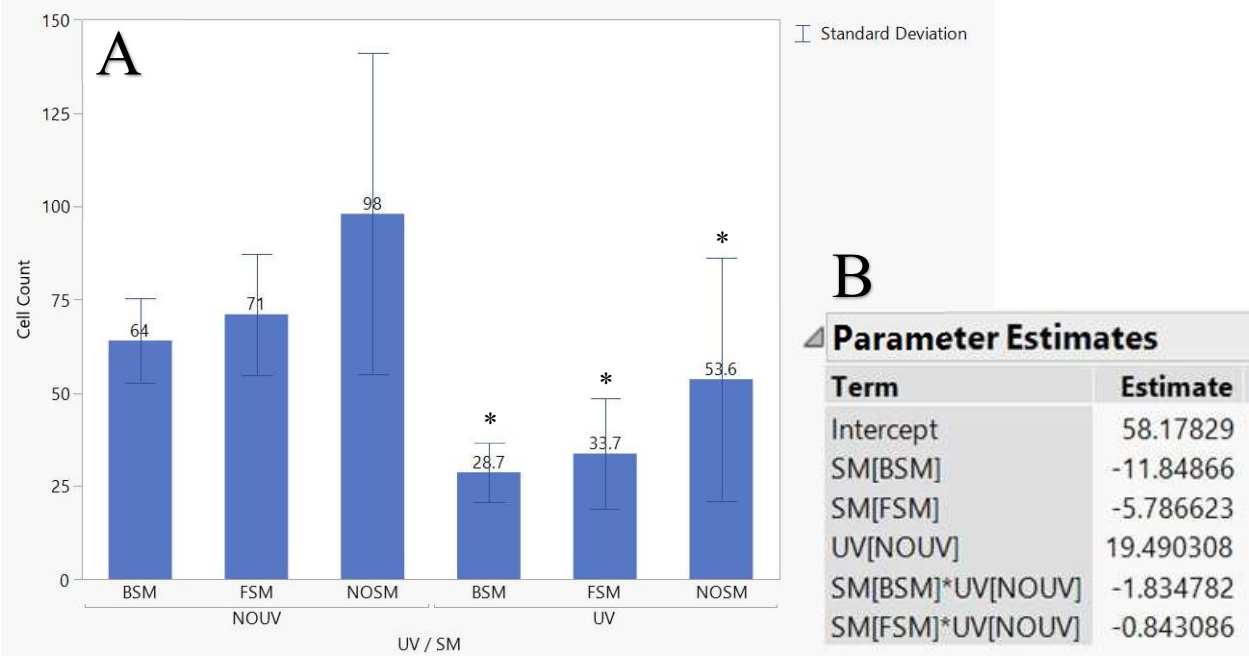

Figure 39: Experiment 7 Cell Count. A. Average cell count separated by sphingomyelin and UV treatments. There was significant evidence * < 0.0001 that there was a difference between number of cell before and after UV irradiation. B. Parameter estimate is the prediction of how the response variable changes for a change in the explanatory variable. * t < 0.0001.

4.7.2.2 P21 Intensity

P21 intensities were separated depending on secondary because overall, Secondary AF 594 appeared dimmer than Secondary AF 488. For both analyses, there was insufficient evidence to reject the hypothesis that there are no differences observed between sphingomyelin and UV treatments, Figure 40. This lack of significance is due a combination of high variability seen by the large standard deviation bars and from the low levels of contrast between the No UV and UV intensities. The largest delta between No UV and UV case was 0.171 meaning measurement needs to be very accurate to capture the true mean difference.

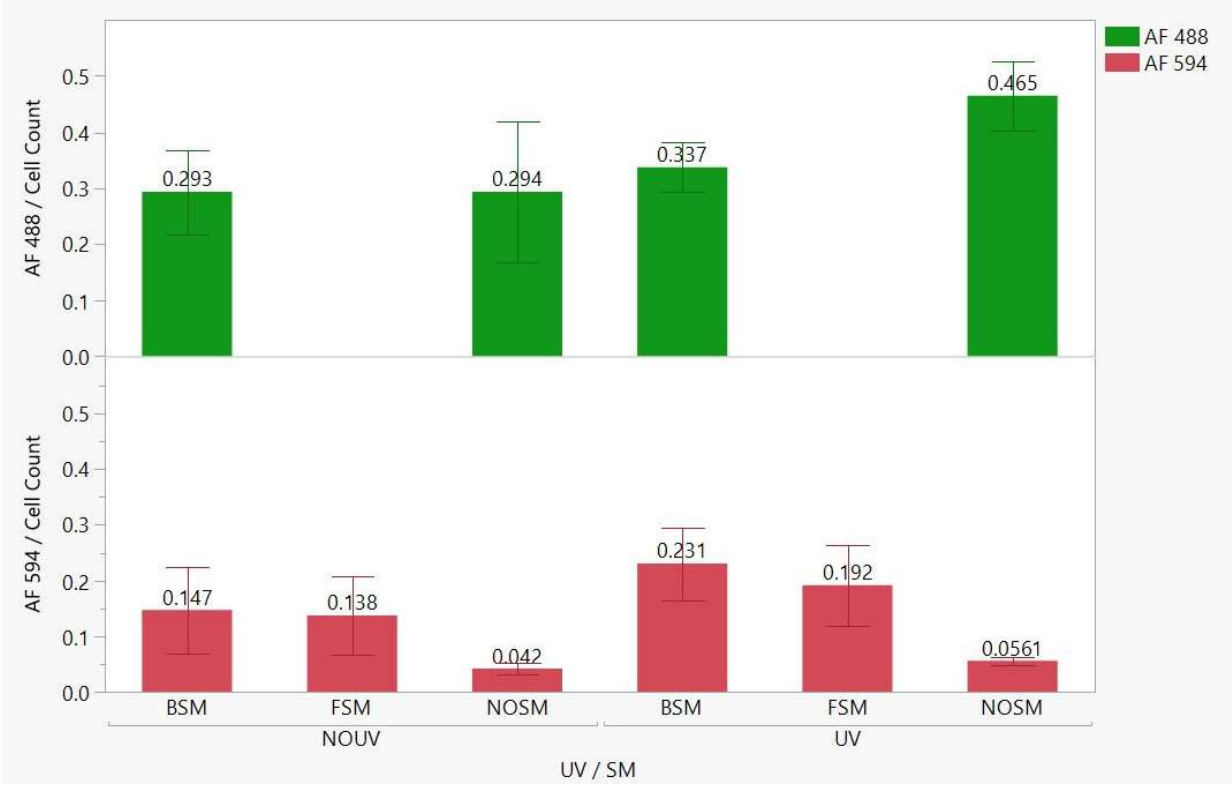

Figure 40: Experiment 7 p21 Intensities. Secondary AF 448 are the green bars (n=20) and Secondary AF 594 are the red bars (n=27).

4.7.2.3 Min and Max Grey Values

Previous filtering minimum and maximum ranges were based on Experiment 1 results (i.e. minimum value should be less than 1 and maximum value should be 255), Section 4.1. However, range should reflect larger data set values. After excluding non-ideal results, summarized in Table 6, a new filtering range was established. Minimum values should continue to be less than 1 and maximum values can have a range from 250 to 255, Figure 41. There appeared to be tendency for max values to reach 255. This max value means that the detector was saturated past the laser's detection limit and was unable to record the true maximum intensity. Tracking minimum and maximum values range ensures that the contrast between images are not abnormal and further efforts should try to prevent oversaturation of intensities.

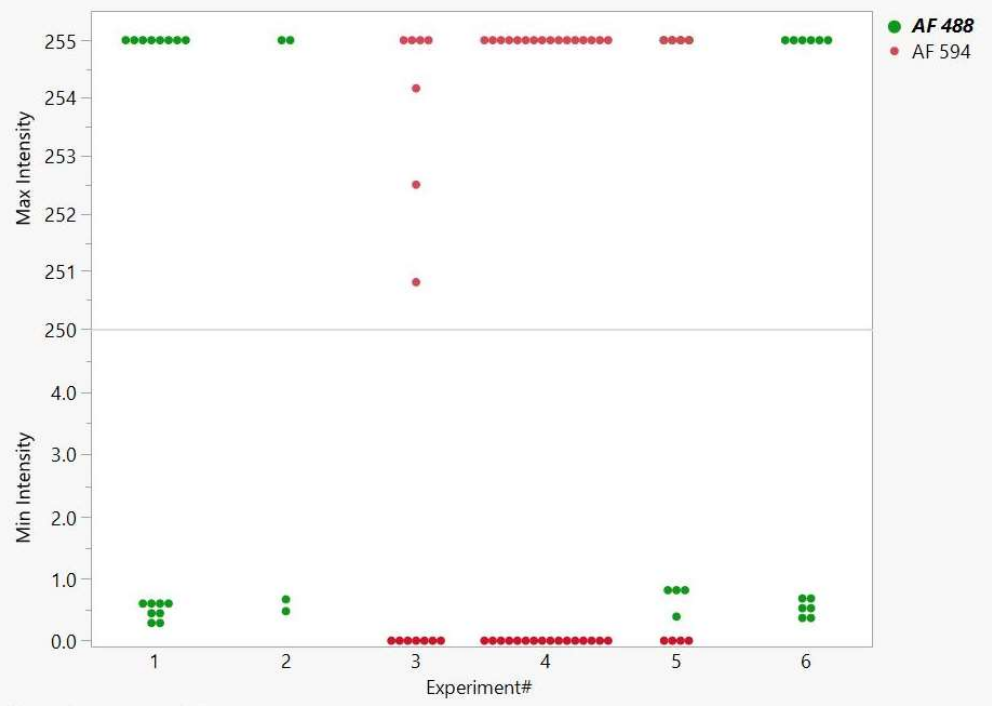

Figure 41: Experiment 7 Minimum and Maximum Values.

4.7.2.4 Circularity

Description of circularity can be found in Table 4. Previously, Experiment 1 showed nuclei circularity was affected by UV irradiation. With the additional experiments, circularity is statistically different between no UV and UV irradiation, Figure 42. It is predicted that average nucleus circularity is 0.73 and decreases by 0.03 when exposed to UV irradiation. Not only does UV kill cells, it can also cause morphological changes in the cell's structure. Circularity of the cell's outer lipid membrane was not analyzed because there was no clear visualization method, however, we can assume morphological changes in the nucleus translates to larger changes of the whole cell. Observationally it was seen that cells incubated with BSM appeared larger and less circular than those treated without. This could contribute to the cell count observed per plate.

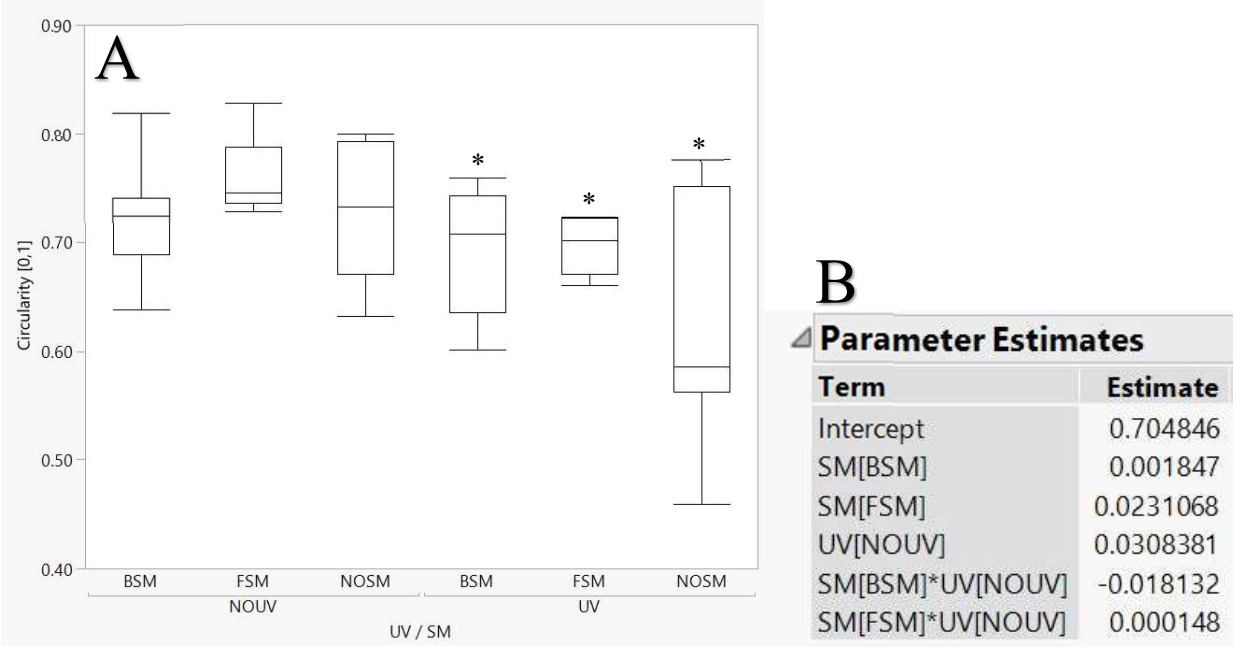

Figure 42: Experiment 7 Nuclei Circularity. A. Boxplot of circularity of nuclei based on sphingomyelin treatment and UV irradiation. There is significant difference between No UV and UV results, *< 0.001. B. Parameter estimate is the prediction of how the response variable changes for a change in the explanatory variable. * t < 0.001.

4.7.2.5 Correlations

Correlation is a measure of how two quantitative variables relate to each other. Variables can be positively correlated if they both increase/decrease at the same time or negatively if they move in opposite directions [72]. Correlation is considered strong when their r value is larger than 0.7. The following 5 quantitative variables were evaluated for correlations: cell count, total area, average size, perimeter^2, and circularity.

Based on the equation for calculating circularity, Equation 3, the following relationships should hold true: circularity directly proportional to average size, circularity inversely proportional to perimeter^2, and average size directly proportional to perimeter^2.

$$Circularity = \frac{4\pi * Area}{Perimeter^2} \qquad \text{(Equation 3) [73]}$$

Note: Average size is equivalent to Area.

The correlation matrix, shown in Figure 43, shows the following strong relationships: cell count α total area, average size α perimeter^2, and perimeter^2 α 1/circularity. A strong correlation between circularity and average size was not observed.

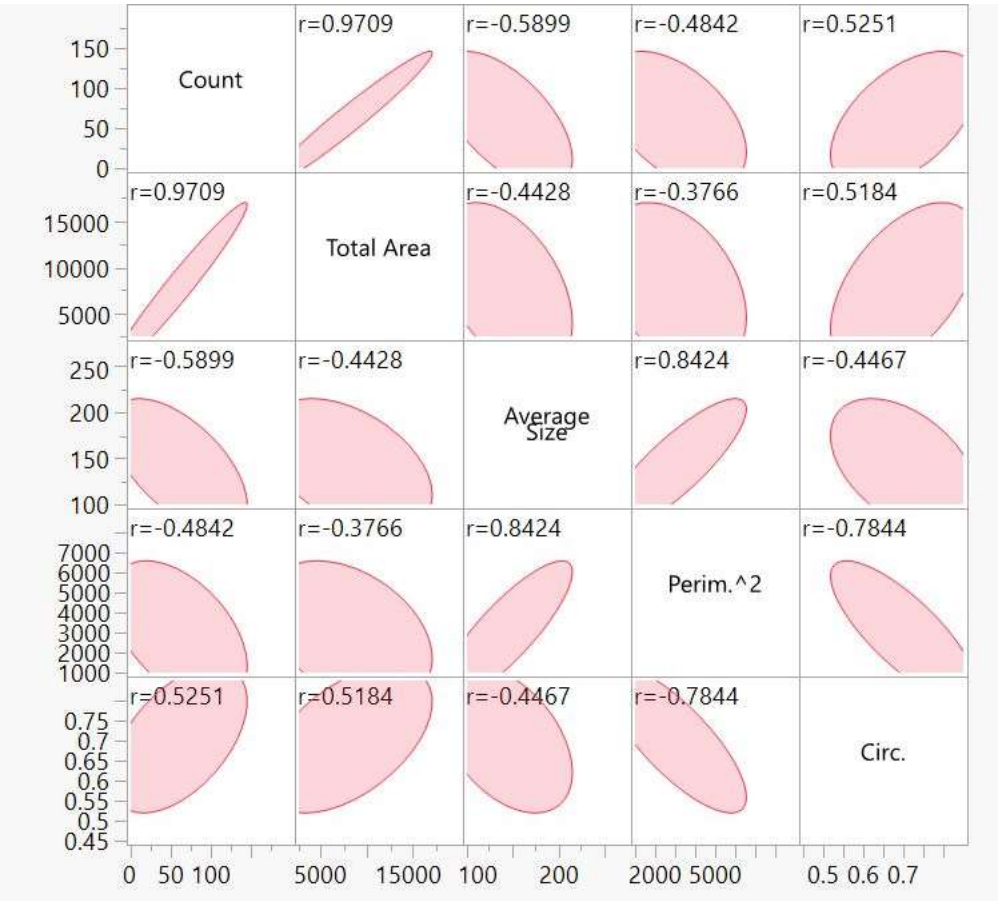

Figure 43: Correlation Matrix. The narrower the ellipse, the more related the variables. Note: These observations relate to the nuclei of each image, not the overall shape of the cell.

4.7.2.6 Sample Size Estimation

Plate standard deviations were previously plotted, and high deviations were removed from analysis, Figure 38. Variance is alternative metric similar to standard deviation; it calculates how varied a sample is and can be calculated manually using Equation 4.

$$s^2 = \frac{\Sigma(X-\bar{X})^2}{N-1}$$ (Equation 4) [74]

Mean and variance of intensities were found to be different depending on secondary used, Figure 44. Secondary AF 488 had a mean of 0.352 with a variance of 0.0127. Secondary AF 594 had a mean of 0.143 with a variance of 0.00754.

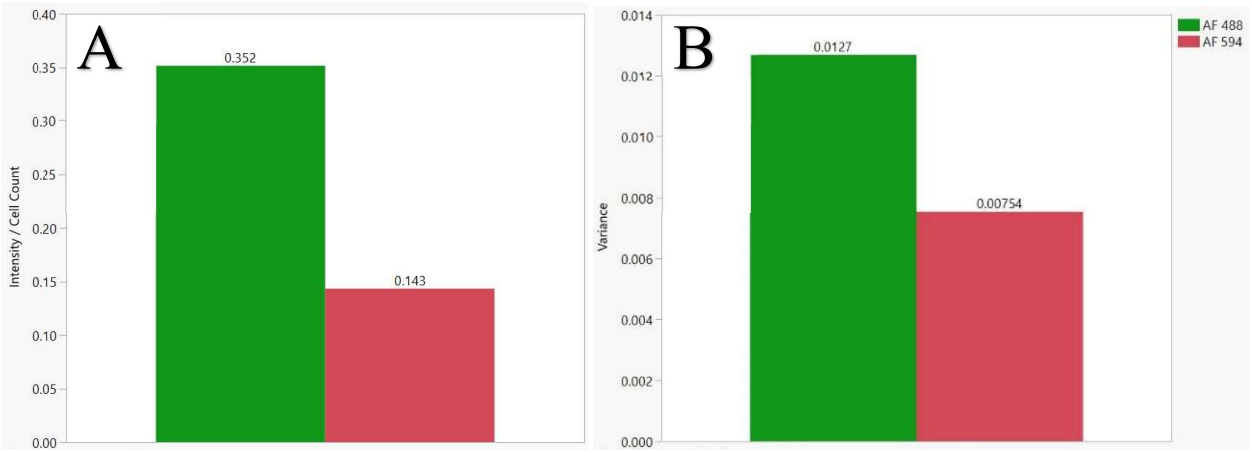

Figure 44: Experiment 7 Mean and Variance of Intensities. A. Mean plate intensities differing by secondary. B. Mean variance of intensities differing by secondary.

An unbiased population variance can be estimated using sample variance obtained from the data, Equation 5.

$$population\ variance = \left(\frac{n}{n-1}\right) * sample\ variance$$ (Equation 5) [75]

Additionally, population standard deviation was estimated using the calculated population variance, Equation 6.

$$standard\ deviation = \sqrt{variance}$$ (Equation 6) [75]

Sample size estimation can be determined using Equation 7.

$$n \geq \left(\frac{critical\ value * standard\ deviation}{level\ of\ error}\right)^2$$ (Equation 7) [74]

Level of error refers to the specificity or accuracy of results. Generally, the level of error is less than 5% of the population parameter or 5% of mean value but can be adjusted based on application. Calculation was done using a max level of error of 5%, 10%, and 15% of the mean.

Table 8 summarizes sample sizes needed for various confidence levels and levels of error. With a specificity of 0.05 and a confidence level of 95%, there was no difference between treatments using Secondary AF 488. Additional testing is needed to decrease the level of error and increase the confidence level. Secondary AF 594 requires much larger sample sizes due its low intensity values.

Table 8: Sample Size Estimation.

Confidence Level	Critical Value		Secondary AF 488		Secondary AF 594	
			Max Level of Error	Sample Size	Max Level of Error	Sample Size
90%	1.645	5% Mean	0.0176	117	0.0072	416
		10% Mean	0.0352	30	0.0143	104
		15% Mean	0.0528	13	0.0215	47
95%	1.96	5% Mean	0.0176	166	0.0072	590
		10% Mean	0.0352	42	0.0143	148
		15% Mean	0.0528	19	0.0215	66
99%	2.575	5% Mean	0.0176	286	0.0072	1018
		10% Mean	0.0352	72	0.0143	255
		15% Mean	0.0528	32	0.0215	114

4.7.3 Discussion

The purpose of this experiment was to understand sources of unexplained variation and to predict how they affected the results. Results from Experiments 1 – 6

were combined and after excluding abnormal plate values, cell nuclei and p21 intensities were analyzed.

Data analysis revealed UV irradiation caused a difference in cell count of about 24%. Images exposed to UV irradiation had approximately 24% less cells than those that did not. The results may be due to a series of factors such as cell growth, harsh treatment, exposure time. This metric could be used to confirm UV irradiation was effectively administered.

Overall, p21 intensities were not statistically different between treatments. This was due to high variation between plates and further work is needed to mimimize this variation. It was observed that Secondary AF 594 had lower contrast than Secondary AF 488. Therefore the use of Secondary AF 488 should be exclusively used because of the following reasons: location of FSM and BSM were documented in Experiment 5 and eliminated the need to use FSM, Secondary AF 488 had higher contast than Secondary AF 594, and Secondary AF 488 requires less concentration than Secondary AF 594 which reduces regent cost and decreases non-specific binding.

Using minimum and maximum intensity values as reference, intensity oversaturation may have contributed to the results. The number of times max values were 255 showed sensitive laser settings were to oversaturation. Additionally, a minimum value range of 0-1 and a maximum value range from 250-255 was established to serve as a quality check for the normality of the images.

Nucleus cicularity was seen to negeatively be impacted by UV irradiation. Because morphological changes of nucleus is expected to be applified in whole cell, UV

irradiation is expected to further affect cell's shape. Using a correlation matrix, the following relationships were confirmed: cell count proportional to total area, nucleus size proportional to nucleus' perimeter^2, and perimeter^2 inversely proportional to nucleus circularity.

Lastly, population standard deviations were estimated using the sample variance to predict number of samples needed for different error and confidence levels, summarized in Table 8. Additional testing is needed to decrease the level of error and increase the confidence level. Secondary AF 594 required much larger sample sizes due its low intensity values.

5 CONCLUSION

Overall, there were a total of 6 experiments and one meta-analysis. All experiments had goals that aligned with one of the three objectives: 1. Observe differences between cells exposed with sphingomyelin versus without 2. Visualize sphingomyelin within the cell and 3. Identify experimental parameters that contribute to variation in results. Further experimentation was halted due to COVID-19; however, additional experiments are outlined below and should be performed when lab resumes. Table 9 summarizes the goals and conclusions obtained from each experiment.

In Experiment 1, the best indicator of cell damage was found to be p21 intensity normalized by cell count. P21 intensity peaked for the No SM + UV treatment and was lower for the BSM + UV treatment. This indicated similar results to previous experimentation that BSM provided some level of photoprotection against UV irradiation. Additional parameters were evaluated; min/max values were thought to help filter abnormal images, and nucleus circularity was found to be affected by treatments.

In Experiment 2, FSM was introduced as an analog to BSM to visualize sphingomyelin within the cell. However, changes due to a new secondary, negatively affected the clarity of the results. Laser settings induced noise to the images and FSM did not show similar results to BSM. This highlighted the need to optimize the new secondary concentration and FSM/BSM incubation time.

Experiment 3 and 4 tried to address the previous concerns. They resulted in an updated protocol that included the following: increased Secondary AF 594 concentration to 1:200, reduced Hoechst concentration to 0.015%, and reduced FSM/BSM incubation

time to 2 hours. All these changes were done to increase signal of p21 intensity and to decrease variation by reducing noise from the external factors.

In Experiment 5, FSM was reevaluated for BSM equivalence. It was concluded BSM and FSM shared no significant differences. This means the location of the FSM and assumed location was consistent to BSM. After analysis of the FSM location, it is proposed that sphingomyelin disrupts well-formed lipid rafts that ultimately reduce p21 upregulation (i.e., less cell damage).

Experiment 6 and 7 attempted to find statistical significance between the treatment groups. Because there were high levels unexplained variation, sample size was too low to find statistical differences. Even though protocol was modified to produce the best images with the lowest variability, there were other sources of variation such as cell growth, equal UV treatment, and other handling differences. Using an estimate of population variance, sample sizes were estimated in Table 8 to conclude significance with varying confidence levels and error.

Lastly in Experiment 7, the nucleus circularity, min/max values, and cell count were reevaluated to determine if a larger sample size observed the same trends. The min and max ranges were slightly modified relaxed, but appropriate quality image check. Additionally, the tendency for max values to be 255 showed how easily oversaturation could occur when adjusting laser settings. A cell count reduction of approximately 24% is an indication that the UV irradiation was effectively administered. Having too low of a cell count reduction could signal not enough irradiation and too high of a reduction could signal the opposite. Nucleus circularity was statistically different pre versus post UV

irradiation. This reduction in circularity may be indicative of lower cell health and could be an additional metric for evaluating cell damage.

Table 9: Summary of Experiments and Results

Experiment	Goal	Conclusions
1. Replication of Previous Experimentation	1: Replicate procedure and compare results. 2: Identify new parameters that introduces variation between treatments.	1: BSM reduced p21 positive intensity post UV irradiation. Results were similar to previous experimentation 2: A variety of new parameters were evaluated. Nucleus circularity was affected by treatments. Additionally, min and max values should filter results that are abnormal.
2. FSM Treatment	1: Replicate FSM procedure 2: Introduce new Secondary AF 594	1: FSM procedure did not yield the same protective effects as BSM. 2: High laser settings for new Secondary AF 594 led to low contrast between treatments. There was a need to optimize for FSM incubation and new Secondary AF 594 concentration.
3. Optimizing New Secondary Concentration	1: Optimize for new Secondary AF 594 2: Evaluate reduction of Hoechst concentration	1: A secondary concentration of 1:200 had the best contrast with the least variability. 2: Hoechst concentration of 0.015% reduced oversaturation of DAPI channel.
4. Optimizing Incubation Time	1: Optimize FSM incubation with new Secondary AF 594 concentration	1: An incubation time of 2 hours had the lowest p21 intensity, lowest variation within treatments, and had no differences between UV and no UV case.
5. FSM Localization	1: Compare FSM with BSM 2: Observe the distribution of FSM within keratinocytes	1: FSM and BSM were comparable as well as they may have protected plates from p21 damage. 2: Profile plot shows globular pockets of fluorescence along the nucleus. After nucleus, intensity radially decreases until it reaches cell's outer membrane. Sphingomyelin disrupts well-formed lipid rafts that ultimately reduces p21 upregulation.
6. Experiment replication with updated protocol	1: Replicate previous experimentation results using new	1: Results were contradictory with previous experimentation. This may be due to abnormality in cell count.

	substrates, materials, and slightly modified procedure 2: Understand variation between experiments	2: There was high variation between experiments.
7. Compiled data	1: Understand inter and intra subject variation 2: Evaluate treatment effects on new parameters and its significance 3: Estimate number of trials needed for statistical significance	1: No statistical significance difference between BSM and No SM, but a slight trend was observed. Large standard deviation between plates as well as between experiments (ie. large intra and inter standard deviation). 2: Min/max values and cell count could serve as quality check to ensure image is not abnormal. UV reduces cell count by approximately 24% and reduces circularity. Circularity correlates with perimeter^2 and average size. Count correlates with Total Area. 3: Table 8 summarizes the number of additional trials needed to reach statistical power using an estimation for variance of the population.

This research was done in an attempt to introduce a novel method for UV protection. Unlike sunscreen, additional safety and efficacy data would not be needed because sphingomyelin is normally found in common foods and is already prevalent in the blood stream. Studies involving lab mice showed consumption of sphingomyelin could inhibit other types of cancer [55], Section 2.8.5. Obtaining quantitative evidence of its photoprotective properties and characterizing its metabolism within keratinocytes are the first steps in developing a drug to ultimately combat skin cancer.

Ideally, to remove the variation observed between experiment, one large study should be conducted using many plates ($n > 30$). However, it poses too much of a strain on the lab's resources. Not only would the lab have to procure large amounts of reagents, there would have to be many people to ensure plates received treatments at the same time

points. Additionally, even if resources such as reagents and personnel were obtained, the limiting factor would be the confocal microscope. It has been shown that the level of p21 intensity decreases as the duration between staining and imaging increases. Currently, it takes approximately 30 minutes to image one plate. This makes the delta large between the first and last plate if more plates were being evaluated.

Therefore, future lab experimentation should focus on further reducing intra-subject variation. Some procedural modifications could be starting experiments at consistent times in the day, monitoring ambient temperature, or implementing tests to check quality of reagents. Other modifications post processing could include filtering for min and max ranges, filtering for abnormal cell count, or using another marker for cell damage that has a higher sensitivity compared to p21. Currently, this thesis addresses the behavior of a monolayer of keratinocytes. Additional efforts of the lab include growing 3D constructs of keratinocytes to further characterize sphingomyelin's effects in a more true, representative state. After effects are confirmed with statistical power, research efforts should focus on developing a method to introduce sphingomyelin to in-vivo models.

BIBLIOGRAPHY

[1] WHO, "Skin cancers," *WHO,* 2017-10-16 14:37:04 2017, doi: /entity/uv/faq/skincancer/en/index.html.

[2] US_FDA, "Sunscreen: How to Help Protect Your Skin from the Sun | FDA," 2020.

[3] A. Turney, "FDA In Brief: FDA announces results from second sunscreen absorption study | FDA," January 21, 2020 2020.

[4] P. Kikas, G. Chalikias, and D. Tziakas, "Cardiovascular Implications of Sphingomyelin Presence in Biological Membranes," (in eng), *Eur Cardiol,* vol. 13, no. 1, pp. 42-5, Aug 2018, doi: 10.15420/ecr.2017:20:3.

[5] R. M. Kandell and S. L. O. California Polytechnic State University, "Assessing the Photoprotective Effects of Fluorescent Sphingomyelin Against UVB Induced DNA Damage in Human Keratinocytes," California Polytechnic State University, San Luis Obispo, 2018.

[6] B. Ogretmen, "Sphingolipid metabolism in cancer signalling and therapy," (in En), *Nature Reviews Cancer,* ReviewPaper vol. 18, no. 1, pp. 33-50, 2017-11-17 2017, doi: doi:10.1038/nrc.2017.96.

[7] T. Abbas and A. Dutta, "p21 in cancer: intricate networks and multiple activities," (in eng), *Nat Rev Cancer,* vol. 9, no. 6, pp. 400-14, Jun 2009, doi: 10.1038/nrc2657.

[8] OpenStax, "5.1 Layers of the Skin," (in en), 1999-2016.

[9] O. L. Initiative. "The Cell | Anatomy and Physiology I." Carnegie Mellon University. https://courses.lumenlearning.com/austincc-ap1/chapter/the-cell/ (accessed.

[10] M. Hoffman, "The Skin (Human Anatomy): Picture, Definition, Function, and Skin Conditions," 2014.

[11] MayoClinic, "Skin cancer - Symptoms and causes," 2020.

[12] Y. Smith, "What is the Dermis?," 2016-12-02 2016.

[13] Y. Smith, "What is the Epidermis?," 2016-11-29 2016.

[14] R. L. Eckert and E. A. Rorke, "Molecular biology of keratinocyte differentiation," (in eng), *Environ Health Perspect,* vol. 80, pp. 109-16, Mar 1989.

[15] "Keratinocytes: Their Purpose, Their Subtypes and Their Lifecycle | Tempo Bioscience." https://www.tempobioscience.com/blog/?p=410 (accessed.

[16] SkinCancerOrg, "Skin Cancer Facts & Statistics - The Skin Cancer Foundation," 2020.

[17] M. P. Hendaria, A. Asmarajaya, and S. Maliawan, "SKIN CANCER," (in id), *E-Jurnal Medika Udayana,* pp. 273-289, 2013 2013.

[18] I. Slamdot, "What's the difference between melanoma and non-melanoma skin cancer? | Premier Surgical Associates," ed, 2016.

[19] R. A. Schwartz, "Basal Cell Carcinoma," (in en), pp. 87-104, 2008.

[20] H. Witmanowski, M. Lewandowska, P. Szychta, S. Sporny, and J. Rykała, "The development of squamous cell carcinoma in a patient after kidney transplantation: a case report," in *Postepy Dermatol Alergol*, vol. 30, no. 1), 2013, pp. 65-71.

[21] R. A. Schwartz, "Squamous Cell Carcinoma," (in en), pp. 47-65, 2008.

[22] L. A. Dourmishev, D. Rusinova, and I. Botev, "Clinical variants, stages, and management of basal cell carcinoma," in *Indian Dermatol Online J*, vol. 4, no. 1), 2013, pp. 12-7.

[23] ACS, "What Is Melanoma Skin Cancer? | What Is Melanoma?," *American Cancer Society,* August 14, 2019 2019.

[24] P. J. Cohen, M. A. Hofmann, W. Sterry, and R. A. Schwartz, "Melanoma," (in en), pp. 152-199, 2008.

[25] K. Grifantini, "How Does Sunscreen Work?," June 25, 2010 2010.

[26] AAD, "Is sunscreen safe?," *American Academy of Dermatology | Association,* 2020.

[27] EWG, "EWG's 2019 Guide to Safer Sunscreens," 2020.

[28] UCAR. "Ultraviolet (UV) Radiation." UCAR Center for Science Education. https://scied.ucar.edu/ultraviolet-uv-radiation (accessed.

[29] M. Vazquez, *UV Radiation, Ozone and Life | SpringerLink*. SpringerLink, 2006.

[30] S. M. Directorate. "Ultraviolet Waves." NASA Science. https://science.nasa.gov/ems/10_ultravioletwaves (accessed.

[31] M. S. Bell, Amber, "Skin and the Effects of Ultraviolet Radiation - Lesson," October 8, 2019 2019.

[32] W. C. Shiel Jr., "Definition of UV radiation," *MedicineNet,* 2017.

[33] ND, "Uses for UV," *Science Learning Hub,* 2017.

[34] R. Hopkins, "How Ultraviolet Light Reacts in Cells," *SciBytes,* February 14, 2015 2015.

[35] M. P. Martin, J. A. Endicott, and M. E. Noble, "Structure-based discovery and development of cyclin-dependent protein kinase inhibitors," (in eng), *Essays Biochem,* vol. 61, no. 5, pp. 439-52, Nov 08 2017, doi: 10.1042/ebc20170040.

[36] M. E. Law, P. E. Corsino, S. Narayan, and B. K. Law, "Cyclin-Dependent Kinase Inhibitors as Anticancer Therapeutics," in *Mol Pharmacol*, vol. 88, no. 5), 2015, pp. 846-52.

[37] Y. Xiong, G. J. Hannon, H. Zhang, D. Casso, R. Kobayashi, and D. Beach, "p21 is a universal inhibitor of cyclin kinases," (in En), *Nature,* OriginalPaper vol. 366, no. 6456, pp. 701-704, 1993, doi: doi:10.1038/366701a0.

[38] B. Alberts, A. Johnson, J. Lewis, M. Raff, K. Roberts, and P. Walter, "Intracellular Control of Cell-Cycle Events," Text 2002 2002, doi: https://www.ncbi.nlm.nih.gov/books/NBK26856/.

[39] S. Waga, G. J. Hannon, D. Beach, and B. Stillman, "The p21 inhibitor of cyclin-dependent kinases controls DNA replication by interaction with PCNA," *Nature,* July 1994 1994, doi: 10.1038/369574a0.

[40] ND, "Caspase 3, the executioner of apoptosis," 2015-11-02 2015.

[41] P. C. Calder, S. o. M. Institute of Human Nutrition, University of Southampton, Southampton S016 7PX, UK, P. Yaqoob, and S. o. F. B. Hugh Sinclair Unit of Human

Nutrition, University of Reading, Reading RG6 6AP, UK, "Lipid Rafts—Composition, Characterization, and Controversies," *The Journal of Nutrition,* vol. 137, no. 3, pp. 545-547, 2007, doi: 10.1093/jn/137.3.545.

[42] T. Kinoshita, "Glycosylphosphatidylinositol (GPI) Anchors: Biochemistry and Cell Biology: Introduction to a Thematic Review Series," in *J Lipid Res*, vol. 57, no. 1), 2016, pp. 4-5.

[43] K. Simons and E. Ikonen, "Functional rafts in cell membranes," (in En), *Nature,* ReviewPaper vol. 387, no. 6633, pp. 569-572, 1997, doi: doi:10.1038/42408.

[44] A. Hainovitz-Friedman, R. N. Kolesnick, and Z. Fuks, "Ceramide signaling in apoptosis," *British Medical Bulletin,* vol. 3, pp. 539 - 553, 1997.

[45] K. I.-B. Kitatani, Jolanta. Hannun,Yusuf A., "The sphingolipid salvage pathway in ceramide metabolism and signaling," *Cellular Signalling,* vol. 20, no. 6, pp. 1010-1018, 2008, doi: https://doi.org/10.1016/j.cellsig.2007.12.006.

[46] B. LR, L. SJ, R. EF, and R. R, "Ceramide Signalling and the Immune Response," *Biochimica et biophysica acta,* vol. 1301, no. 3, 06/11/1996 1996, doi: 10.1016/0005-2760(96)00004-5.

[47] ND, "What is NF-κB pathway?," *MBInfo | Defining Mechnobiology,* 2020.

[48] A. Fischbeck, M. Krüger, N. Blaas, and H.-U. Humpf, "Analysis of Sphingomyelin in Meat Based on Hydrophilic Interaction Liquid Chromatography Coupled to Electrospray Ionization−Tandem Mass Spectrometry (HILIC-HPLC-ESI-MS/MS)," (in EN), research-article October 6, 2009 2009, doi: 10.1021/jf9025376.

[49] "Milk SM | Avanti Polar Lipids." https://avantilipids.com/product/860063 (accessed.

[50] ND, "Artificial fluorescent membrane lipid shows active role in living cells," *Nanowerk News,* Jun 05, 2017 2017.

[51] "C6-NBD Sphingomyelin | Avanti Polar Lipids." https://avantilipids.com/product/810218 (accessed.

[52] SkinCancerOrg, "Can Your Diet Help Prevent Skin Cancer? - The Skin Cancer Foundation," 2017-06-08 2017.

[53] H. Vesper *et al.*, "Sphingolipids in Food and the Emerging Importance of Sphingolipids to Nutrition," *The Journal of Nutrition,* vol. 129, no. 7, pp. 1239-1250, 1999, doi: 10.1093/jn/129.7.1239.

[54] Å. N. Lena Nyberg, Pia Lundgren, Rui-Dong Duan, "Localization and capacity of sphingomyelin digestion in the rat intestinal tract," vol. 8, ed: The Journal of Nutritional Biochemistry, 1997, pp. 112-118.

[55] D. L. Dillehay *et al.*, "Dietary Sphingomyelin Inhibits 1,2-Dimethylhydrazine-Induced Colon Cancer in CF1 Mice," *The Journal of Nutrition,* vol. 124, no. 5, pp. 615-620, 1994, doi: 10.1093/jn/124.5.615.

[56] D. F. Birt *et al.*, "Inhibition of skin carcinomas but not papillomas by sphingosine, N-methylsphingosine, and N-acetylsphingosine," (in en), *http://dx.doi.org/10.1080/01635589809514690,* other 4 Aug 2009 2009, doi: Nutrition and Cancer, Vol. 31, No. 2, 1998, pp. 119-126.

[57] K. Campbell and S. L. O. California Polytechnic State University, "The use of Sphingomyelin to protect against UV induced DNA damage in Human Keratinocytes," California Polytechnic State University, San Luis Obispo, 2015.

[58] T. M. Fraser and S. L. O. California Polytechnic State University, "Molecular Dynamics of p21 and Fluorescent Sphingomyelin in Keratinocytes Exposed to UVB," California Polytechnic State University, San Luis Obispo, 2018.

[59] ND. "Fixation (histology)." Wikipedia. https://en.wikipedia.org/wiki/Fixation_(histology) (accessed.

[60] ND, "Preparing Fixed Cells for Labeling - US," *ThermoFisher Scientific,* 2020.

[61] "Preparing Fixed Cells for Labeling - US," 2020.

[62] ND. "Differences Between Primary and Secondary Antibodies | ProSci Inc." ProSci. https://www.prosci-inc.com/resources/antibody-development-guide/primary-and-secondary-antibodies/ (accessed.

[63] J. Sedgewick, *Scientific Imaging with Photoshop: Methods, Measurement, and Output*. Peachpit, 2008.

[64] ND. "Macro Language." https://www.ncbi.nlm.nih.gov/pubmed/ (accessed.

[65] ND. "Analyze Menu." Background is Lighter. https://www.ncbi.nlm.nih.gov/pubmed/ (accessed.

[66] Stephanie, "Nested Model, ANOVA and Factors: Simple Definitions and Examples," 2017-09-18 2017.

[67] H. Ahmadi, "NESTED DESIGNS," Apr 27, 2015 2015.

[68] ND. "Blurring images - Image Processing with Python." DataCapentry. https://datacarpentry.org/image-processing/06-blurring/ (accessed.

[69] ND. "GaussianBlur (ImageJ API)." https://www.ncbi.nlm.nih.gov/pubmed/ (accessed.

[70] K. De Guzman and S. L. O. California Polytechnic State University, "Protective Effects of Sphingomyelin against UV Photodamage in Human Keratinocytes," California Polytechnic State University, San Luis Obispo, 2013.

[71] Z. Achay and S. L. O. California Polytechnic State University, "PROTECTIVE EFFECTS OF MILK PHOSPHOLIPIDS AGAINST UV PHOTODAMAGE IN HUMAN SKIN EQUIVALENTS," California Polytechnic State University, San Luis Obispo, 2011.

[72] G. T. Kurian. "Correlation." CQ Press. (accessed.

[73] "Analyze Menu." Background is Lighter. https://www.ncbi.nlm.nih.gov/pubmed/ (accessed.

[74] M. Stansberry, "How to Determine Sample Size With Mean & Standard Deviation," March 14, 2018 2018.

[75] E. W. Weisstein, "Sample Variance," (in en), Text 2003-07-02 2003, doi: https://mathworld.wolfram.com/SampleVariance.html.

APPENDICES

A. P21 Protocol

P21 Protocol

Materials:
Triton X, 1% goat serum, PBS, P21 primary (rabbit), formaldehyde, Hoechst stain, 2ndary antibody (goat anti rabbit)

Procedure:

Day 1

1. Remove media and wash once with PBS. All washes should be done gently.
2. Fix cell with 3.7% formaldehyde and let sit for 15 minutes.
3. Do three washes and add 0.1% triton X solution to each well. Let sit for 20 minutes.
4. Do 3 more washes and add 1% blocking solution to the cells.
5. Let the blocking stay on overnight. It is ok to let blocking stay on for longer, though this is not true for the primary.
6. Do three more washes with PBS.
7. Add p21 primary antibody (1/400 dilution with PBS).
8. Let p21 sit for about 9 hours. **Letting the primary stay on for too long may negatively affect performance**.
9. Later the same day or the next day, remove P21 and wash three times with PBS.
10. Add secondary (1/400 dilution) to each well.
11. Let incubate (in darkness) for an hour. Wash three times with PBS.
12. Add 0.05% Hoechst stain to each well. Leave in darkness for 15 minutes.
13. Wash three times and be sure to leave enough PBS to cover the each well. This allows for best imaging.
14. Wrap in foil and image with confocal.

Washing and Solution Preparation:
Make sure to slowly drop PBS on the cells during washes. Rough treatment will damage cells and reduce confluency.
Makes sure to slowly pull liquid out of the well in a corner. Going too fast or touching the bottom of the well will pull cells out.
Pipetting small volumes should have the user slowly pull liquid in and out of the pipet (2-3 times) to ensure accurate volumes.
Always invert your stock and created solutions before using. This ensures that the active molecules reach the cells.

Imaging:
The images should allow for clear identification of p21 positive or negative cells.

B. ImageJ Macros

P21 Intensity

1. In ImageJ, click on Analyze > Set Measurements…

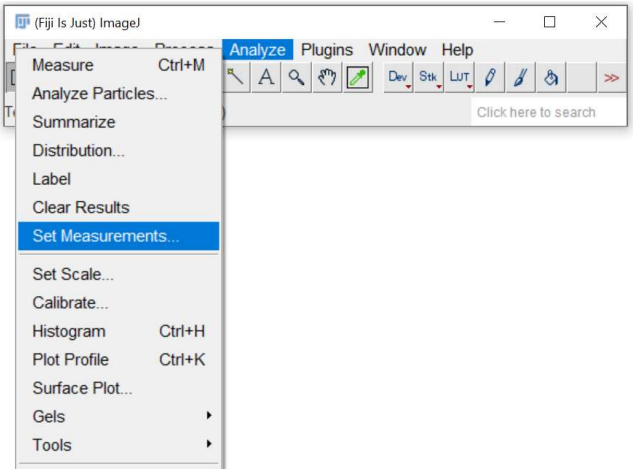

2. In Set Measurements, select Area, Standard Deviation, Min & Max gray value, and Mean gray value.

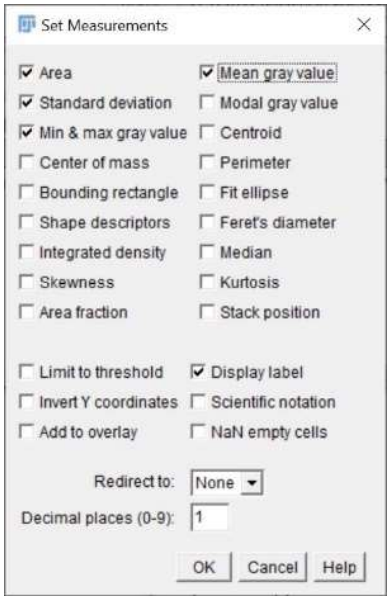

3. Open .oibs with separate channels and keep track the channel of interest (ie. the p21 channel).
4. Open macro and run program.

```
setOption("ScaleConversions", true);

run("8-bit");

run("8-bit");

run("Measure");

close();
```

Note: Functions can be repeated more than once and executed on the same macro.

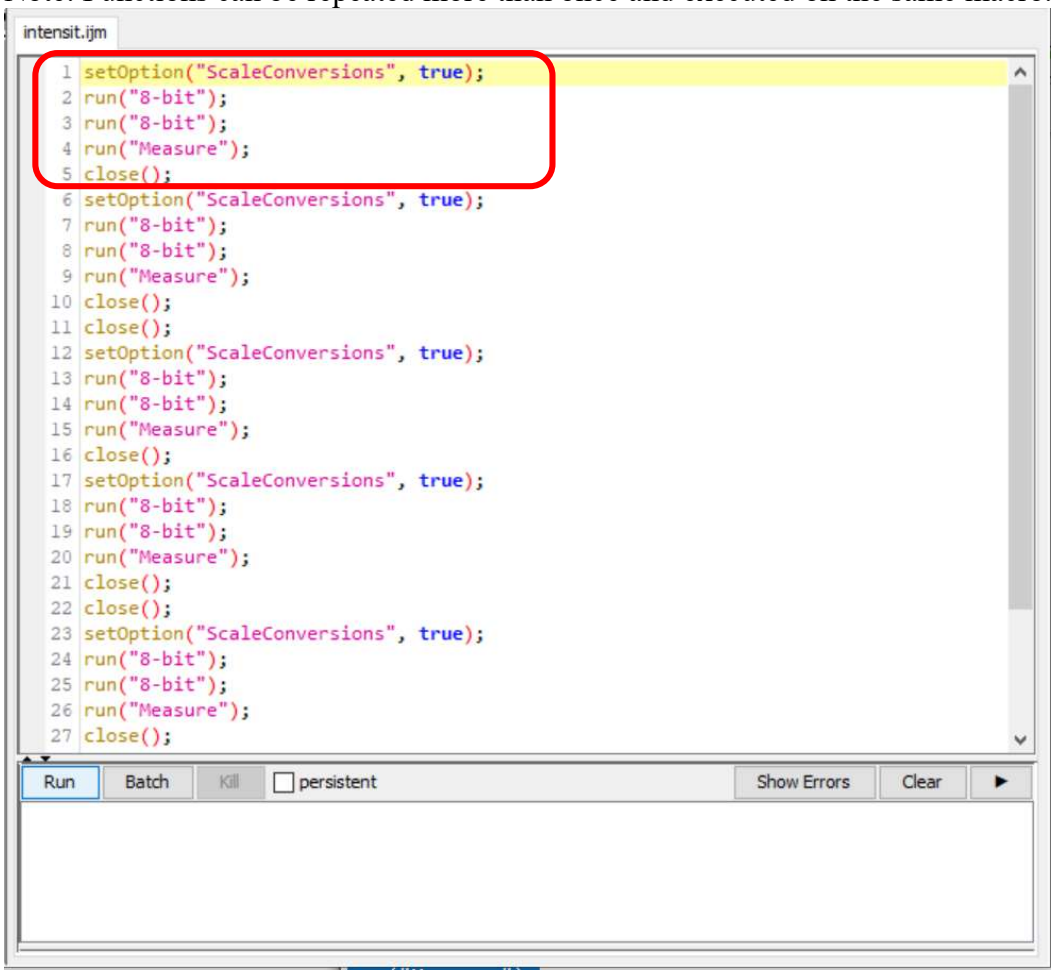

5. Results should appear in a results window and can be saved as a .csv.

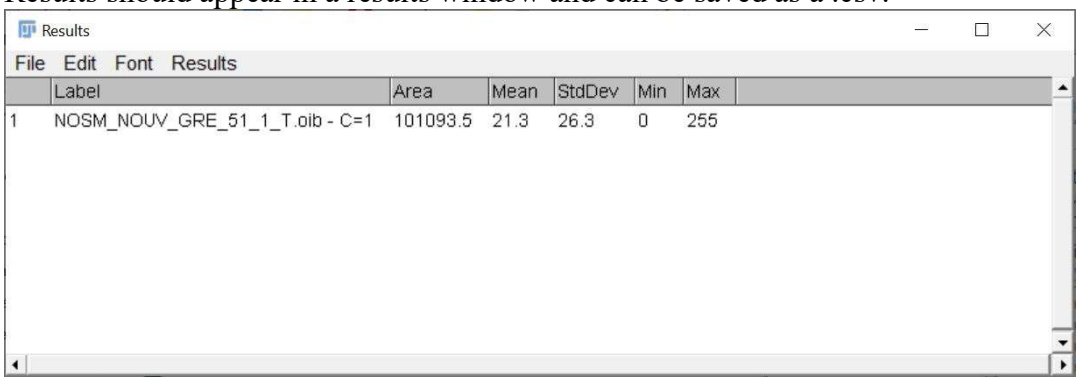

Cell Count

1. In ImageJ, click on Analyze > Set Measurements…

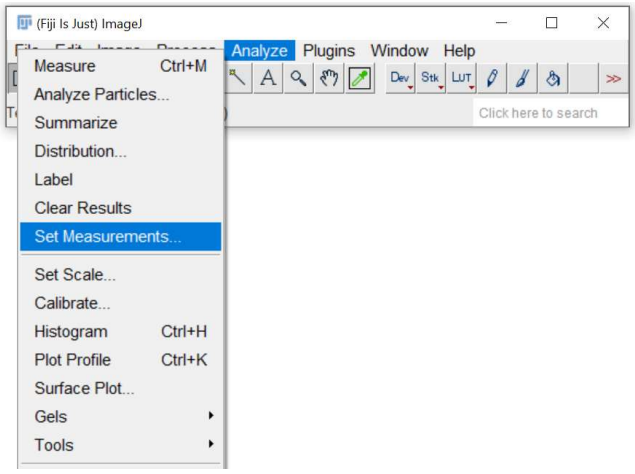

2. In Set Measurements, select Area, Standard Deviation, Shape descriptors, and Perimeter.

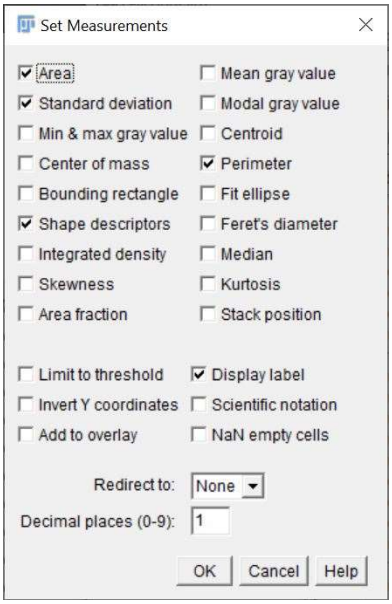

3. Open .oibs with separate channels and keep track the channel of interest (ie. the DAPI channel).

4. Open macro and run program.

```
run("Subtract Background...", "rolling=90");

setOption("ScaleConversions", true);

run("8-bit");

run("8-bit");

run("Convert to Mask");

run("Analyze Particles...", "size=90-Infinity pixel show=Outlines display exclude clear summarize");

run("Measure");

close();
```

Note: Functions can be repeated more than once and executed on the same macro.

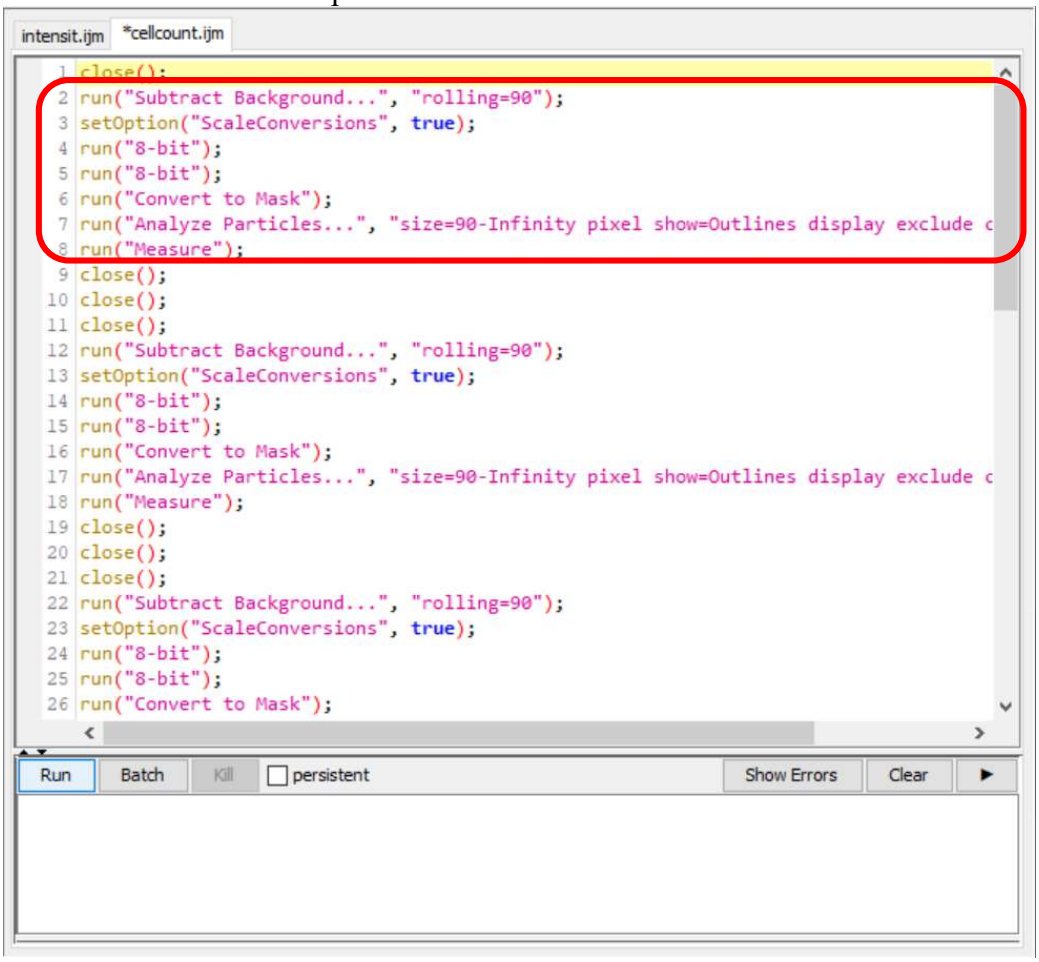

5. Results should appear in a results window and can be saved as a .csv.